

DISCRETE FEYNMAN-KAC CORRECTORS

Mohsin Hasan^{1,2*}, **Viktor Ohanesian**^{3*}, **Artem Gazizov**⁴,
Yoshua Bengio^{1,2}, **Alán Aspuru-Guzik**^{5,6,7}, **Roberto Bondesan**³,
Marta Skreta^{1,2}, **Kirill Neklyudov**^{1,2,8}

¹Université de Montréal, ²Mila, ³Imperial College London, ⁴Harvard University,
⁵University of Toronto, ⁶Vector Institute, ⁷NVIDIA, ⁸Institut Courtois

ABSTRACT

Discrete diffusion models have recently emerged as a promising alternative to the autoregressive approach for generating discrete sequences. Sample generation via gradual denoising or demasking processes allows them to capture hierarchical non-sequential interdependencies in the data. These custom processes, however, do not assume a flexible control over the distribution of generated samples. We propose DISCRETE FEYNMAN-KAC CORRECTORS, a framework that allows for controlling the generated distribution of discrete masked diffusion models at inference time. We derive Sequential Monte Carlo (SMC) algorithms that, given a trained discrete diffusion model, control the temperature of the sampled distribution (i.e. perform annealing), sample from the product of marginals of several diffusion processes (e.g. differently conditioned processes), and sample from the product of the marginal with an external reward function, producing likely samples from the target distribution that also have high reward. Notably, our framework does not require any training of additional models or fine-tuning of the original model. We illustrate the utility of our framework in several applications including: efficient sampling from the annealed Boltzmann distribution of the Ising model, improving the performance of language models for code generation and amortized learning, as well as reward-tilted protein sequence generation.

1 INTRODUCTION

The success of diffusion models in continuous domains, such as the generation of images (Rombach et al., 2022), videos (Wang et al., 2023; Blattmann et al., 2023), or 3D protein structures (Abramson et al., 2024; Watson et al., 2023), has motivated their application to discrete data spaces. Indeed, modeling discrete data such as text or biological sequences using diffusion processes is a promising direction since they do not rely on sequential token generation as with autoregressive models, which can impose arbitrary orderings on data (e.g., molecular structures and protein sequences (Lee et al., 2025; Alamdari et al., 2023)), or can suffer from exposure biases that limit long-horizon planning or reversal reasoning in natural language domains (Berglund et al., 2023; Nie et al., 2025).

Discrete diffusion is a general framework that defines a Continuous-Time Markov Chain (CTMC) process that progressively transforms data to a tractable distribution through a series of random transitions, and then learns to reverse this process and recover the original data distribution (Campbell et al., 2022; Lou et al., 2024; Sahoo et al., 2024; Shi et al., 2024). Furthermore, using external classifiers (Vignac et al., 2022; Nisonoff et al., 2024; Tang et al., 2025) or correction schemes (Nisonoff et al., 2024; Gruver et al., 2023) one can efficiently sample from various conditional distributions, e.g. conditioning on desired target properties of a protein (Gruver et al., 2023).

Most practical applications, however, require producing novel and task-specific generations rather than precise recreation of the training data. To produce novel generations, most generative models rely either purely on generalization abilities (Brown et al., 2020; Saharia et al., 2022) or on external reward functions in different forms (DeepSeek-AI, 2025; Rector-Brooks et al., 2024; Singhal et al., 2025). Furthermore, it has been shown that one can control the distribution of the produced samples

*Equal contribution.

Correspondence to mohsin.hasan@mila.quebec, v.ohanesian24@imperial.ac.uk

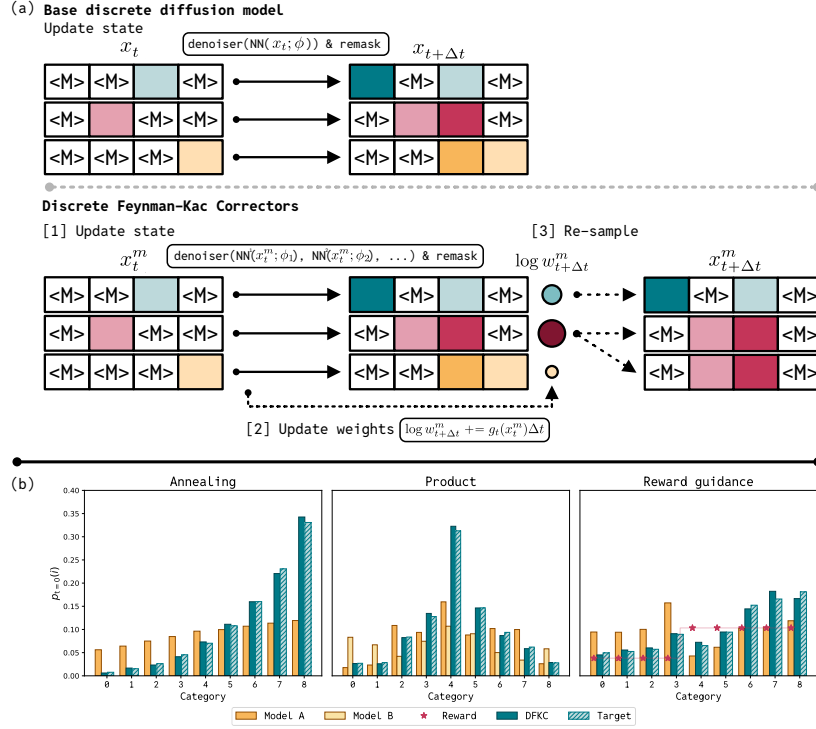


Figure 1: DISCRETE FEYNMAN-KAC CORRECTORS allow sampling from annealed distributions, product (or geometric average), and reward-tilted distributions. Panel (a) depicts the schematic of DFKC compared to the standard inference of masked discrete diffusion. Panel (b) demonstrates how DFKC, given trained discrete diffusion models and the reward function, samples from modified distributions at inference time.

by running task-specific Sequential Monte Carlo (SMC) methods at inference time (Skreta et al., 2024; 2025; He et al., 2025). In particular, Skreta et al. (2025) proposes the Feynman-Kac Correctors, which enable sampling from annealed densities ($p_t^{\text{anneal}}(x) \propto p_t(x)^\beta$) or a product of multiple densities ($p_t^{\text{prod}}(x) \propto \prod_{i=1}^M p_t^i(x)$) by simulating weighted stochastic differential equations (SDEs) with SMC resampling. This framework, however, is derived and presented only for the Fokker-Planck equation and does not directly apply to the discrete diffusion models, which are described by CTMC.

We cover the existing literature gap by introducing DISCRETE FEYNMAN-KAC CORRECTORS (DFKC) — a principled framework enabling the control of discrete diffusion models at inference time (see Figure 1). In particular, given a trained discrete diffusion model with marginals $p_t(i)$ or several models with $p_t^1(i), p_t^2(i), \dots$ (or the same model with different conditions $p_t(i|c_1), p_t(i|c_2), \dots$), we modify the inference process to sample from the: (i) temperature annealed version of the marginals $p_t^{\text{anneal}}(i) \propto p_t(i)^\beta$, where β is the inverse temperature (ii) product of corresponding marginals $p_t^{\text{prod}}(i) \propto p_t^1(i)p_t^2(i)$ (iii) geometric average of the marginals $p_t^{\text{avg}}(i) \propto p_t^1(i)^\gamma p_t^2(i)^{(1-\gamma)}$ (iv) reward-tilted marginals $p_t^{\text{reward}}(i) \propto p_t(i) \exp(\beta_t r(i))$, where $r(i)$ is the external reward function.

Our contribution is two-fold, we establish the theoretical framework that applies to general CTMC processes and we illustrate its utility with multiple applications on different domains. In particular, for each part of the framework, we choose the most promising and fitting applications: (i) we demonstrate that DFKC allows for efficient inference-time control of the temperature when sampling the configurations of the Ising model, which can be used as an efficient sampling algorithm (Akhound-Sadegh et al., 2025) (ii) we demonstrate that applying DFKC to a language model can be used to improve performance on programming tasks (with annealing) and allow scaling to larger prompts for amortized learning (using products) (iii) finally, we demonstrate how DFKC can be used to generate realistic protein sequences (Wang et al., 2024b) while optimizing external reward functions.

2 BACKGROUND

We consider continuous-time Markov chains (CTMC) or jump processes on discrete state spaces. Namely, every variable x_t can take values in the range $0, \dots, m$, and the time t is in the interval $t \in$

[0, 1]. All such processes are described by the Forward Kolmogorov Equation (FKE) (Kolmogoroff, 1931), which is why our main results are stated in terms of these equations.

For discrete diffusion, we consider the specific case of masked diffusion processes and reserve a specific ‘mask’ state m into the set of discrete states. We simulate the diffusion process by discretizing the corresponding FKE in time, and use standard notation: $\text{Cat}(x | \pi)$ denotes the categorical distribution with probabilities π , and δ_{ij} is the Kronecker symbol.

2.1 SIMULATING FORWARD KOLMOGOROV EQUATION (FKE)

The forward Kolmogorov equation for continuous-time Markov chains describes the evolution of the transition probability as follows

$$\frac{\partial p(x_s = j | x_t = i)}{\partial s} = \sum_k A_s(k, j) p(x_s = k | x_t = i), \quad A_s(k, j) := \left. \frac{\partial p(x_t = j | x_s = k)}{\partial t} \right|_{t=s}.$$

In practice, FKE can be used to parameterize the time-evolution of the marginals by specifying the rate matrix $A_t(i, j)$ and the initial boundary condition $p_{t=0}(i) := p(x_0 = i)$. In this case, the change of the marginals is defined as follows

$$\frac{\partial p_t(i)}{\partial t} = \sum_j A_t(j, i) p_t(j), \quad \sum_j A_t(i, j) = 0, \quad A_t(i, i) \leq 0, \quad A_t(i, j) \geq 0, \quad \forall i \neq j, \quad (1)$$

where we introduce constraints on the family of the possible matrices $A_t(i, j)$ according to the definition of the rate matrix.

Fortunately, this constraints can be easily satisfied by parameterizing only the off-diagonal terms of the matrix $A_t(i, j)$ and defining the diagonal term $A_t(i, i)$ as the negative sum over the off-diagonal.

$$\frac{\partial p_t(i)}{\partial t} = \sum_{j \neq i} (A_t(j, i) p_t(j) - A_t(i, j) p_t(i)). \quad (2)$$

To draw samples from $p_t(i)$ one can draw samples from $p_0(i)$ and simulate FKE by discretizing it in time. Namely, at every iteration, one samples from the following conditional probability

$$p(x_{t+dt} = j | x_t = i) = \delta_{ij} + A_t(i, j) dt + o(dt), \quad \text{i.e. } x_{t+dt} \sim \text{Cat}(x_{t+dt} = j | \delta_{ij} + A_t(i, j) dt). \quad (3)$$

In this work, we are interested in FKEs of the particular form

$$\frac{\partial p_t(i)}{\partial t} = \sum_{j \neq i} (A_t(j, i) p_t(j) - A_t(i, j) p_t(i)) + p_t(i) (g_t(i) - \mathbb{E}_{p_t(i)} g_t(i)), \quad (4)$$

where the first term corresponds to the standard FKE as in Equation (2) and the second term corresponds to re-weighting of the samples according to some function $g_t(i)$. In general, the second term does not extend the family of jump processes described by the standard FKE because it can be incorporated into the rate matrix (see Section B.1). However, importantly, this term allows using the Feynman-Kac formula as stated in the following theorem (see the derivation in Section B.2).

Theorem 2.1. [Feynman-Kac Formula] *For the forward Kolmogorov equation from Equation (4) describing the time-evolution of the marginals $p_t(i)$ with the rate matrix $A_t(i, j)$ and weights $g_t(i)$, $\bar{g}_t(i) = g_t(i) - \sum_k p_t(k) g_t(k)$*

$$\begin{aligned} \mathbb{E}_{p_T(x)} \phi(x) &= \lim_{dt \rightarrow 0} \sum_{x_T} \dots \sum_{x_0} \phi(x_T) p(x_T | x_{T-dt}) \dots p(x_{dt} | x_0) \exp \left(\sum_{t=0}^T dt \bar{g}_t(x_t) \right) p_0(x_0) \\ &= \mathbb{E}_{X_{0:T}} \exp \left(\int_0^T dt \bar{g}_t(X_t) \right) \phi(X_T) \propto \mathbb{E}_{X_{0:T}} \exp \left(\int_0^T dt g_t(X_t) \right) \phi(X_T), \end{aligned} \quad (5)$$

where the expectation on the right hand side is taken w.r.t. trajectories $X_{0:T}$ defined as the limit of the transitions from Equation (3).

In particular, to simulate Equation (4), one can extend the states x_t with the weights w_t and jointly simulating the following equations

$$\text{for } x_t = i, x_{t+dt} \sim \text{Cat}(x_{t+dt} = j \mid \delta_{ij} + A_t(i, j)dt), \log w_{t+dt} = \log w_t + g_t(i)dt. \quad (6)$$

Finally, the weighted samples (x_T^k, w_T^k) can be used for the Self-Normalized Importance Sampling (SNIS) estimator or the corresponding empirical measure

$$\mathbb{E}_{p_T(i)} \phi(i) \approx \sum_k \frac{w_T^k}{\sum_j w_T^j} \phi(x_T^k), \quad p_T(i) \approx \sum_k \frac{w_T^k}{\sum_l w_T^l} \delta_{ix_T^k}. \quad (7)$$

2.2 DISCRETE MASKED DIFFUSION

Analogously to continuous-space diffusion models (Song et al., 2021), the discrete diffusion models operate by mapping the data distribution $p_0(i)$ to a simple marginal $p_1(i)$ and then simulating the reverse process. In particular, masked diffusion models define a conditional probability $p(x_s = j \mid x_t = i)$ as a probability of switching from any state to the m -th state, which denotes the utility ‘mask’ state. These conditional probabilities can be described using the following formula (see the derivation in Section B.3), which yields the corresponding rate matrix.

$$p(x_s = j \mid x_t = i) = \left(1 - \frac{\alpha_s}{\alpha_t}\right) \delta_{mj} + \frac{\alpha_s}{\alpha_t} \delta_{ij}, \quad A_t(i, j) = \frac{1}{\alpha_t} \frac{\partial \alpha_t}{\partial t} (\delta_{ij} - \delta_{mj}) \quad (8)$$

In general, the reverse-time process with the marginals $q_\tau(i) := p_{1-\tau}(i)$ is also described by FKE

$$\frac{\partial q_\tau(i)}{\partial \tau} = \sum_{j \neq i} (B_\tau(j, i) q_\tau(i) - B_\tau(i, j) q_\tau(i)), \quad B_\tau(i, j) = A_{1-\tau}(j, i) \frac{p_{1-\tau}(j)}{p_{1-\tau}(m)}, \quad (9)$$

where $A_t(i, j)$ and $B_\tau(i, j)$ are the rate matrices of the forward-time and reverse-time processes correspondingly (see Section B.4). Note that here and throughout the paper we define only the off-diagonal terms of the matrices and the diagonal is automatically defined as $B_\tau(i, i) = -\sum_{j \neq i} B_\tau(i, j)$.

Finally, one can sample from the data distribution $p_{t=0}(i)$ by first generating samples from $p_{t=1}(i)$ and then simulating the reverse-time FKE from Equation (9). For the masked diffusion process from Equation (8) the off-diagonal elements of the rate matrix are

$$B_\tau(i, j) = -\delta_{mi} \frac{1}{\alpha_t} \frac{\partial \alpha_t}{\partial t} \frac{p_t(j)}{p_t(m)} = -\delta_{mi} \frac{1}{\alpha_t} \frac{\partial \alpha_t}{\partial t} \left(\delta_{mj} + \frac{\alpha_t}{1 - \alpha_t} p(x_0 = j \mid x_t = m) \right), \quad (10)$$

where the last equality (shown in Shi et al. (2024)) comes from the relation between the ratio of probabilities $p_t(j)/p_t(m)$ and the conditional de-masking probability $p(x_0 = j \mid x_t = m)$ (see details in Section B.5). In practice, one can parameterize either ‘score’ $s_t(m, j; \theta) = p_t(j)/p_t(m)$ (as suggested in Lou et al. (2024); Benton et al. (2024)) or the de-masking probability $p(x_0 = j \mid x_t = m) = (1 - \delta_{mj}) \text{softmax}(\text{NN}(x_t; \theta))_j$ (as suggested in (Shi et al., 2024)). For our purposes, these parameterizations are equivalent. Furthermore, both these parameterizations can be learned by maximizing the same Evidence Lower Bound (ELBO) objective.

Finally, all the derivations seamlessly transfer to any number of dimensions (see Section B.6). In particular, one can define the masking process independently over the dimensions, and obtain the following off-diagonal elements of the reverse-time rate matrix

$$B_t(i_1 \dots i_d, j_1 \dots j_d) = -\frac{1}{\alpha_t} \frac{\partial \alpha_t}{\partial t} \frac{p_t(j_1 \dots j_d)}{p_t(i_1 \dots i_d)} \sum_{k=1}^d \prod_{l \neq k} \delta_{j_l i_l} \delta_{m i_k}, \quad [i_1 \dots i_d] \neq [j_1 \dots j_d], \quad (11)$$

which are not zero only when all the coordinates except one match. Thus, one can parameterize the reverse-time process by predicting $(m - 1)d$ values, where d is the number of dimensions (or sequence length) and $(m - 1)$ is the vocabulary size for each discrete variable.

3 DISCRETE FEYNMAN-KAC CORRECTORS

In this section, we introduce DISCRETE FEYNMAN-KAC CORRECTORS—a framework that allows for inference-time control of discrete diffusion models. Our derivations proceed in the same fashion for all the cases. First, we consider general CTMC processes with given rate matrices and initial conditions, which induce corresponding marginals. Applying different transformations to these marginals (annealing, product, geometric averaging, reward-tilting), we define new CTMC processes and derive corresponding rate matrices. These derivations state our main results in the most general form. Further, we proceed by applying these derivations to the masked diffusion processes and demonstrate that the transformed processes can be efficiently simulated without any additional training or finetuning. For each case, as we demonstrate, one requires only the ratio of marginal densities, or, equivalently, the denoising conditional probability, which are used for parameterizing the reverse-time process as shown in Equation (10).

3.1 TEMPERATURE ANNEALING¹

First, we present the general result that holds for the forward Kolmogorov equation with arbitrary rate matrix $A_t(i, j)$. Since we do not assume any structure of the matrix, it is easier to reason in terms of Equation (2), i.e. using only the off-diagonal entries assuming that the diagonal elements are chosen correspondingly to define the correct rate matrix. The annealed FKE is as follows.

Theorem 3.1. [Temperature Annealing] *Consider the forward Kolmogorov equation from Equation (2) describing the time-evolution of the marginals $p_t(i)$ with the rate matrix $A_t(i, j)$. For the temperature annealed marginals $q_t(i) \propto p_t(i)^\beta$, the following equation holds*

$$\frac{\partial q_t(i)}{\partial t} = \sum_{j \neq i} \left(A_t^{\text{anneal}}(j, i) q_t(j) - A_t^{\text{anneal}}(i, j) q_t(i) \right) + q_t(i) (g_t(i) - \mathbb{E}_{q_t(j)} g_t(j)), \quad (12)$$

$$\text{where } A_t^{\text{anneal}}(i, j) := \beta A_t(i, j) \frac{p_t^{1-\beta}(i)}{p_t^{1-\beta}(j)}, \quad g_t(i) := \sum_{j \neq i} (A_t^{\text{anneal}}(i, j) - \beta A_t(i, j)). \quad (13)$$

Thus, the annealed FKE relies on the rate matrix $A_t(i, j)$ of the original process and the ratio of marginal probabilities $p_t(i)/p_t(j)$, which are readily available for a trained model of the masked diffusion process. The following corollary presents the rate matrix and the weighting function for the reverse-time masked diffusion process.

Corollary 3.2. [Annealed Masked Diffusion] *For the rate matrix of the reverse-time masked diffusion from Equation (10), Theorem 3.1 yields the following off-diagonal elements of the rate matrix and the corresponding weight function*

$$B_\tau^{\text{anneal}}(i, j) = -\delta_{mi} \frac{\beta}{\alpha_t} \frac{\partial \alpha_t}{\partial t} \frac{p_t^\beta(j)}{p_t^\beta(m)}, \quad g_\tau(i) = \delta_{mi} \frac{\beta}{\alpha_t} \frac{\partial \alpha_t}{\partial t} \sum_j \left(\frac{p_t(j)}{p_t(m)} - \frac{p_t^\beta(j)}{p_t^\beta(m)} \right). \quad (14)$$

This corollary demonstrates that both the new rate matrix and the weights can be efficiently evaluated using the ratio of the marginals, which is used in practice to parameterize the reverse process (see Equation (10)). In more detail, one can obtain the new rate matrix by simply scaling it by β and raising the probability ratio to the power β

$$\frac{p_t^\beta(j)}{p_t^\beta(m)} = \delta_{mj} + \frac{\alpha_t^\beta}{(1 - \alpha_t)^\beta} \exp(\beta \log p(x_0 = j | x_t = m)), \quad (15)$$

which corresponds to multiplying the logits of the denoising model by β besides adjusting the schedule dependent coefficients. Finally, the weighting term can be easily obtained by the summation of the probability ratios $p_t(j)/p_t(m)$ over j , which corresponds to the summation over the different coordinates of the network output and does not require additional function evaluations.

¹See Section C.1 for the proofs

3.2 PRODUCT AND GEOMETRIC AVERAGING²

Sampling from the product of marginals can be interpreted as generating samples that are likely according to several models at the same time. Intuitively, all the models must “unanimously agree” on the sample being likely since zero probability of one of the models renders the entire product to be zero (Hinton, 1999). In what follows, we formalize this collaborative generation process as the process with marginals proportional to the product of marginals of different CTMC processes and state it in the general case with arbitrary rate matrices. For simplicity, here, we present the results for the product of two marginals and postpone the general formulation for geometric average of any number of the marginals to Theorem C.3 and Theorem C.4 in Section C.3.

Theorem 3.3. [Product of FKEs] *Consider two forward Kolmogorov equations (from Equation (2)) with different rate matrices $A_t^1(i, j)$ and $A_t^2(i, j)$ describing the evolution of marginals $p_t^1(i)$ and $p_t^2(i)$. For the product of marginals $q_t(i) \propto p_t^1(i)p_t^2(i)$, the following equation holds*

$$\begin{aligned} \frac{\partial q_t(i)}{\partial t} &= \sum_{j \neq i} \left(A_t^{\text{prod}}(j, i)q_t(j) - A_t^{\text{prod}}(i, j)q_t(i) \right) + q_t(i)(g_t(i) - \mathbb{E}_{j \sim q_t(j)}g_t(j)), \quad (16) \\ A_t^{\text{prod}}(i, j) &:= A_t^1(i, j) \frac{p_t^2(j)}{p_t^2(i)} + A_t^2(i, j) \frac{p_t^1(j)}{p_t^1(i)}, \quad g_t(i) := \sum_{j \neq i} \left(A_t^{\text{prod}}(i, j) - A_t^1(i, j) - A_t^2(i, j) \right). \end{aligned}$$

Importantly, the new rate matrix and the weighting terms are defined in terms of both rate matrices $A_t^1(i, j)$ and $A_t^2(i, j)$ and the ratios of probabilities $p_t^1(i)/p_t^1(j)$ and $p_t^2(i)/p_t^2(j)$. All these quantities are readily available in the masked diffusion models. To be precise, we present the corresponding reverse-time rate matrix and the weighting term in the following corollary.

Corollary 3.4. [Product of Masked Diffusions] *For the rate matrix of the reverse-time masked diffusion from Equation (10), Theorem 3.3 yields*

$$B_{\tau}^{\text{prod}}(i, j) = -2\delta_{mi} \frac{1}{\alpha_t} \frac{\partial \alpha_t}{\partial t} \frac{p_t^1(j)}{p_t^1(m)} \frac{p_t^2(j)}{p_t^2(m)}, \quad g_{\tau}(i) = \frac{\delta_{mi}}{\alpha_t} \frac{\partial \alpha_t}{\partial t} \sum_j \frac{p_t^1(j)}{p_t^1(m)} + \frac{p_t^2(j)}{p_t^2(m)} - 2 \frac{p_t^1(j)}{p_t^1(m)} \frac{p_t^2(j)}{p_t^2(m)}$$

According to these formulas, both the rate matrix and the weights can be efficiently evaluated with a single forward pass through each network.

3.3 REWARD-TILTED MARGINALS³

Generative modeling allows optimizing the external reward functions $r(i)$ while staying within the data distribution $p_{t=0}(i)$ to avoid over-optimization and collapsing to degenerate solutions. Usually it is formalized as sampling from the reward-tilted distribution $p_{t=0}(i) \exp(r(i))$, which we discuss in this section. The following result modifies any CTMC process to sample from the reward-tilted distribution. Note that we derive formulas for the off-diagonal elements of the rate matrix.

Theorem 3.5. [Reward-tilted FKE] *Consider the forward Kolmogorov equation from Equation (2) describing the time evolution of the marginals $p_t(i)$ with the rate matrix $A_t(i, j)$. For the reward-tilted marginals $q_t(i) \propto p_t(i) \exp(\beta_t r(i))$, the following equation holds*

$$\frac{\partial q_t(i)}{\partial t} = \sum_{j \neq i} \left(A_t^{\text{reward}}(j, i)q_t(j) - A_t^{\text{reward}}(i, j)q_t(i) \right) + q_t(i)(g_t(i) - \mathbb{E}_{q_t(j)}g_t(j)), \quad (17)$$

$$A_t^{\text{reward}}(i, j) := A_t(i, j) \frac{\exp(\beta_t r(j))}{\exp(\beta_t r(i))}, \quad g_t(i) := \sum_{j \neq i} \left(A_t^{\text{reward}}(i, j) - A_t(i, j) \right) + \frac{\partial \beta_t}{\partial t} r(i). \quad (18)$$

Note that the obtained formulas depend only on the reward function and the rate matrix of the original process. Applying this result to the masked diffusion we obtain the following corollary.

²See Section C.2 for the proofs

³See Section C.4 for the proofs

Algorithm 1: Generation using DISCRETE FEYNMAN-KAC CORRECTORS

Input: corresponding rate matrix $B_\tau(i, j)$ and weight function $g_\tau(i)$, number of samples K

- 1 $x_{\tau=0}^k \sim p_{t=1}(i)$; /* initialize with noise */
- 2 $w_{\tau=0}^k = 1/K$; /* uniform weights */
- 3 **for** $\tau = 0, \dots, 1$ **do**
- 4 $x_{\tau+d\tau}^k \sim \text{Cat}(x_{\tau+d\tau}^k = j \mid \delta_{ij} + B_\tau(i, j)d\tau)$, for $x_\tau^k = i$; /* update state */
- 5 $\log w_{\tau+d\tau}^k = \log w_\tau^k + g_\tau(i)d\tau$; /* update weights */
- 6 **if** resample **then**
- 7 $w_{\tau+d\tau}^k = w_{\tau+d\tau}^k / (\sum_l w_{\tau+d\tau}^l)$; /* re-normalize weights */
- 8 $x_{\tau+d\tau}^k = x_{\tau+d\tau}^l$, $l \sim \text{Cat}(l \mid w_{\tau+d\tau})$; /* re-sample indices */
- 9 $w_{\tau+d\tau}^k = 1/K$; /* re-initialize weights */

Output: weighted set of samples $\{(x_{\tau=1}^k, w_{\tau=1}^k)\}_{k=1}^K$

Corollary 3.6. [Reward-tilted Masked Diffusion] *For the rate matrix of the reverse-time masked diffusion from Equation (10), Theorem 3.5 yields*

$$B_\tau^{\text{reward}}(i, j) = -\delta_{mi} \frac{1}{\alpha_t} \frac{\partial \alpha_t}{\partial t} \frac{p_t(j)}{p_t(m)} \frac{\exp(\beta_t r(j))}{\exp(\beta_t r(m))}, \quad (19)$$

$$g_\tau(i) = \frac{1}{\alpha_t} \frac{\partial \alpha_t}{\partial t} \delta_{mi} \sum_j \left(\frac{p_t(j)}{p_t(m)} - \frac{p_t(j)}{p_t(m)} \frac{\exp(\beta_t r(j))}{\exp(\beta_t r(m))} \right) + \frac{\partial \beta_t}{\partial t} r(i). \quad (20)$$

Note that evaluating $B_\tau^{\text{reward}}(i, j)$ requires computing the reward function at all the states j we can transition to from mask m . Furthermore, computing $g_t(i)$ requires the summation of the reward over all such states j , which, depending on the application, might be computationally expensive. To avoid these extra computations one could potentially use alternative functions evaluating the difference in the rewards on the transitions from m to j , i.e. $r(j) - r(m)$. However, we leave this as a future work.

4 EXPERIMENTS

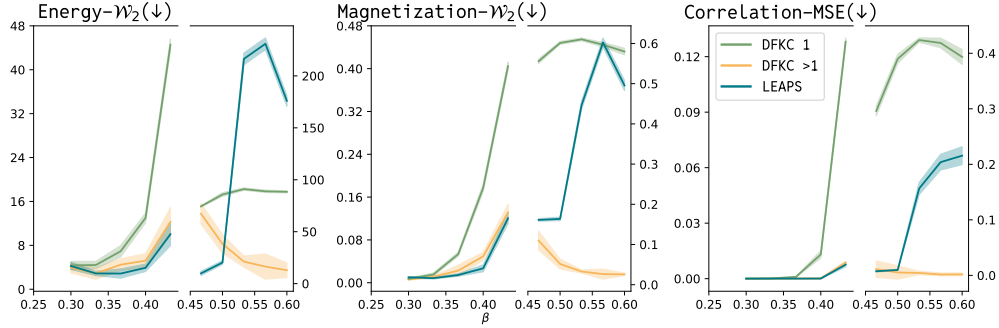
In this section, we demonstrate the utility of the proposed DISCRETE FEYNMAN-KAC CORRECTORS on several applications using modern discrete diffusion models. Each experiment is aimed at illustrating one of the introduced processes: annealing, geometric averaging, reward-tilting.

Despite different domains and processes, the generation process always follows the same procedure described in Alg. 1. Namely, for the corresponding rate matrix $B_\tau(i, j)$ and weight function $g_\tau(i)$ (see Section 3 for their definitions), the inference procedure generates a batch of samples x_τ^k together with their weights w_τ^k . In practice, we always perform resampling in between the update steps using SNIS. Thus, DFKC not only changes the generation of individual samples by changing the rate matrix $B_\tau(i, j)$ but also introduces "interactions" between samples through re-weighting and re-sampling. In Section A.1, we provide the explicit state and weight update rules for sampling from different target densities and show how these discrete updates correspond to the continuous formulation of Skretta et al. (2025).

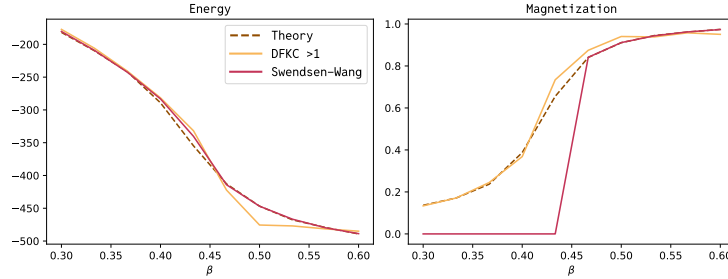
4.1 ANNEALING THE ISING MODEL

Table 1: Sampling task for Ising model with performance measured by mean \pm standard deviation over 3 seeds. The starting temperature for DFKC is shown in brackets. The DDM samples are generated with a discrete diffusion model trained at those corresponding target temperatures.

Target β	Method	Energy- $\mathcal{W}_2(\downarrow)$	Magnetization- $\mathcal{W}_2(\downarrow)$	Correlation-MSE (\downarrow)
0.4	DFKC(0.3)	14.24 ± 3.11	0.256 ± 0.052	0.041 ± 0.013
	DDM	69.38 ± 4.25	0.889 ± 0.063	0.172 ± 0.021
0.3	DFKC(0.2)	33.38 ± 0.46	0.031 ± 0.011	0.023 ± 0.007
	DDM	35.14 ± 0.63	0.046 ± 0.012	0.014 ± 0.009



(a) 2-Wasserstein metric for energy and magnetization distributions and MSE for spin-spin correlation. All metrics are computed between samples from DFKC variants or LEAPS and samples from Swendsen-Wang algorithm. The β used for training DFKC is 0.3. Note that the plots include a break at β_{crit} , and the y -axes use different scales on either side of β_{crit} to make differences in magnitude visible.



(b) Average energy and magnetization over varying β for DFKC, and Swendsen-Wang, compared to theoretical values. Training β for DFKC is 0.3.

Figure 2: Results for annealing on the Ising model.

We apply Theorem 3.1 for annealing the Boltzmann distribution of the Ising model configurations. Namely, the probability distribution of states σ is given as

$$p_\beta(\sigma) = \frac{1}{Z_\beta} e^{-\beta H(\sigma)}, \quad Z_\beta = \sum_\sigma e^{-\beta H(\sigma)}, \quad \text{where } H(\sigma) = - \sum_{i,j} J_{ij} \sigma_i \sigma_j - \sum_i h_i \sigma_i. \quad (21)$$

We generate a training dataset at a fixed β by running the Swendsen-Wang algorithm (Swendsen & Wang, 1987) and train a discrete masked-diffusion model. We set $J_{ij} = 1$ and $h_i = 0$ on a 16×16 lattice with periodic boundary conditions. The diffusion model is parameterized using the UNet architecture. We assess method performance by comparing the distributions of key observables, specifically energy and magnetization. To examine the fidelity of local structures, we compute spin–spin correlations as a function of distance, excluding boundary spins and evaluating correlations along lattice rows. Finally, we evaluate the mean squared error (MSE) between the generated correlation profiles and the ground-truth.

We train the diffusion model at $\beta = 0.3$ and demonstrate that DFKC allows for the efficient control of temperature at inference time in the range $\beta \in [0.3, 0.6]$, with critical point $\beta_{\text{crit}} \approx 0.4407$. As a baseline, we consider a guidance method, which ignores the weights of the generated samples. In addition, a comparison with LEAPS (Holderrieth et al., 2025) is provided. Note that the released LEAPS model is trained on the annealing path $\pi_t(\sigma) \propto \exp(-t \beta_{\text{crit}} H(\sigma))$ for $t \in [0, 1]$, so we do not expect it to work reliably for $\beta > \beta_{\text{crit}}$, and instead expect it to sample only within the range of temperatures it was trained on. Notably, our temperature annealing method, being training-free, allows for sampling beyond the critical temperature. The results in Figure 2a validate this perspective. Additionally, in Figure 2b we plot the mean energy and magnetization obtained by varying β using our method, and observe that it closely follows theoretical results.

In Table 1, we demonstrate that collecting the data at a high temperature and annealing the trained model to the low temperature is more efficient than collecting data and training the model directly at a low temperature. In particular, we fix the number of energy evaluations for the dataset collection and

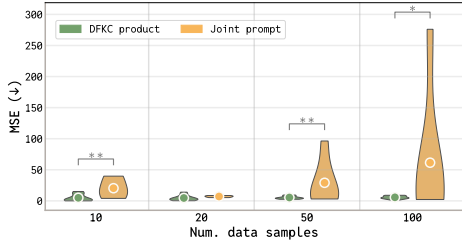


Figure 3: Amortized learning task: Mean squared error (MSE) between predicted and true parameters reported for DFKC (1 and 5 samples), and joint prompting, across different dataset sizes. ** indicates $p \leq 0.02$, * indicates $p \leq 0.05$ (one-sided Student’s t -test).

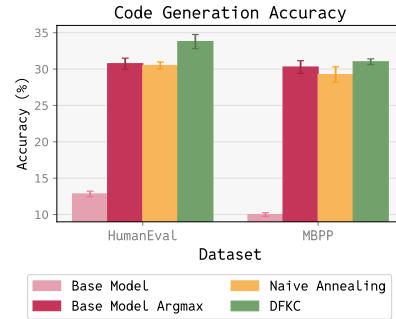


Figure 4: Accuracy on coding tasks, with standard error reported over 5 seeds.

can either allocate this budget for training the discrete diffusion model (DDM) directly on the target temperature, or for training it a higher temperature and then using DFKC to reduce the temperature to the target. To conduct this comparison, we used 10,000 samples following a long burn-in period of Glauber dynamics, which requires lengthy chains to reduce correlations. Additional details of the experiments are included in Section D.1.

4.2 PRODUCTS AND ANNEALING FOR LANGUAGE MODELLING

We evaluate the ability of DFKC to improve performance on text generation tasks by evaluating the annealing formula (from Theorem 3.1) for code generation, and the product formula from Theorem 3.3 for amortized learning. For both tasks, we use the pretrained LLaDA-8B-Instruct as our (masked) diffusion model (Nie et al., 2025).

Code Generation. Recent work argues that annealing an existing model to sample higher likelihood points can result in better performance on various mathematical or coding tasks (Huang et al., 2024). Inspired by this line of work, we investigate the applicability of our annealing method as an inference time strategy for improving accuracy on coding tasks. We anneal the model with parameter β and evaluate its accuracy in solving a diverse set of programming problems in the HumanEval and MBPP datasets (Chen et al., 2021; Austin et al., 2021). We compare with sampling the most likely token at each step (“Argmax” sampling), as well as sampling with inverse-temperature β (“Naive Annealing”). The results are reported in Figure 4, which demonstrate that DFKC obtains a higher accuracy than other sampling methods. Additional details are included in Section D.3.

Amortized Learning. Given a dataset of examples $\mathcal{X} = \{(x_i, y_i)\}_{i=1}^N$, and a parametric model $f_\theta(x)$, we wish to use the language model to infer parameters θ which fit the data. This requires sampling from the posterior distribution over parameters $p(\theta|\mathcal{X})$. However, unlike more classical statistical methods, we wish to perform this computation solely through the text interface of the language model, similar to the setting of (Requeima et al., 2024; Mittal et al., 2025). Namely we set \mathcal{X} as our prompt, and ask the model to sample parameters θ . We partition the dataset into K equal subsets $\mathcal{X} = \bigcup_{k=1}^K \mathcal{X}_k$, and note that for a uniform prior, the posterior factors as $p(\theta|\mathcal{X}) \propto \prod_{k=1}^K p(\theta|\mathcal{X}_k)$. This justifies applying our method, with each factor in the product conditioned on a different subset of the data $C_k = \mathcal{X}_k$. We evaluate this task on a synthetic dataset generated using a noisy linear predictor $f_\theta(x) = \theta_1 x + \theta_0 + \epsilon$ $\epsilon \sim \mathcal{N}(0, 0.1^2)$. We use $K = 5$ subsets, and report our results for the mean-squared error (to the true parameters) across larger datasets \mathcal{X} in Figure 3. From our results, we can see that as the length and complexity of the prompt increases, the joint prompt degrades in performance, compared to the more stable performance of the DFKC product. We also see that using more samples in our method improves performance slightly over 1 sample. This is also validated by an ablation over the number of SMC samples in Figure A1. Additional details and results are included in Section D.2. In Section D.4, we present a related experiment which applies the product formulation of our method for generating stories adhering to a set of constraints.

4.3 GUIDING PROTEIN SEQUENCE GENERATION WITH EXTERNAL REWARDS

Finally, we investigate the utility of DFKC in the setting of unconditional *de novo* protein sequence generation. Protein language models (PLMs) have emerged as powerful tools for modeling the

Table 2: Evaluation for reward-guided protein sequence generation (over 5 seeds).

	Reward $\log r(x)$ (↑)	Diversity		Structural confidence			Novelty	
		Seq. div. (↑)	Max. cluster (↑)	pLDDT (↑)	pTM (↑)	Frac. pLDDT > 0.7 (↑)	Max TM (↓)	Frac. TM < 0.5 (↑)
Task: unconditional generation								
Base [unguided]	-4.3266 ± 0.3190	0.7729	0.3571	0.5941 ± 0.1525	0.2609 ± 0.1452	0.2714	0.6789	0.0500
DG-Exact (Nisonoff et al., 2024)	-1.8831 ± 0.0979	0.7649	0.3333	0.5918 ± 0.1671	0.2671 ± 0.1571	0.3200	0.6547	0.1300
FK Steering (Singhal et al., 2025)	-2.7762 ± 0.1160	0.6171	0.0733	0.5494 ± 0.1408	0.1912 ± 0.0845	0.2133	0.5992	0.1837
DFKC [ours]	-1.6551 ± 0.0952	0.7077	0.1067	0.6005 ± 0.1840	0.2860 ± 0.1677	0.3600	0.6573	0.1443
Task: thermostability								
Base [unguided]	-0.6590 ± 0.0229	0.7729	0.3571	0.5941 ± 0.1525	0.2609 ± 0.1452	0.2714	0.6789	0.0500
DG-Exact (Nisonoff et al., 2024)	-0.6131 ± 0.0191	0.7860	0.3571	0.6088 ± 0.1500	0.2695 ± 0.1550	0.3214	0.6976	0.1111
FK Steering (Singhal et al., 2025)	-0.5841 ± 0.0192	0.7513	0.2733	0.5704 ± 0.1534	0.2246 ± 0.1087	0.2333	0.6559	0.1429
DFKC [ours]	-0.5316 ± 0.0153	0.7618	0.3200	0.5875 ± 0.1517	0.2468 ± 0.1387	0.2533	0.6490	0.2043

complex relationships between protein sequence, structure, and function (Lin et al., 2023; Madani et al., 2023), but controlling their outputs remains a significant challenge. To encourage generation of sequences that resemble natural proteins, we guide sampling with rewards that measure sequence plausibility. We consider two reward settings: (i) the likelihood under a PLM, and (ii) the predicted thermostability of the sequence. The likelihood reward is motivated by the fact that PLMs capture evolutionary constraints and assign higher probability to "natural-like" sequences, a property that has been successfully leveraged to steer generation toward functional and biologically viable proteins (Ertelt et al., 2024; Emami et al., 2023; Notin et al., 2023). The thermostability reward reflects that high stability is a desirable property of natural proteins, correlating with improved folding, robustness, and mutational tolerance. For likelihood evaluation we use the masked language model ESM2-650M (Lin et al., 2023), and for thermostability we use a fine-tuned version of DPLM-650M (Wang et al., 2024a).

We generate sequences using DPLM-650M, a discrete diffusion model that produces protein sequences by progressively unmasking amino acid tokens (Wang et al., 2024a). To guide generation, we set the reward appropriately and apply Theorem 3.5. Table 2 presents the rewards and additional metrics for sequences sampled using our method, for both tasks. The table also compares our method with other guidance-based techniques: FK Steering (using the base model as a proposal) (Singhal et al., 2025), and DG-Exact, the exact guidance approach of Nisonoff et al. (2024). In the guided setting, we note that the single-sample variant of DFKC is equivalent to DG-Exact, and observe that using multiple samples yields notable improvements in mean reward compared to both unguided DPLM sampling and guidance without resampling. These results highlight the effectiveness of our resampling procedure in enhancing desired properties of generated sequences. For likelihood based sampling, our method generates more designable sequences, at the cost of diversity, while for thermostability it maintains similar performance to the base model across other metrics. DG-Exact requires $O(V)$ reward evaluations (with vocabulary size V) for each inference step, while FK Steering performs inference with M samples in parallel. Our method uses both strategies, with run-time similar to DG-Exact (due to parallel computation over M). The combination allows for substantial reward improvement, and makes the method useful for tasks where additional inference compute can be spent to obtain higher quality samples. Additional experimental details and results are included in Section D.5.

5 RELATED WORK

Reward Fine-tuning. These methods often assume an external reward function $r(x)$ and adjust the pretrained model’s parameters using reinforcement learning algorithms, with the goal of sampling from the product $r(x)q_t(x)$. Several of these works are applicable to discrete diffusion models (Venkatraman et al., 2024; Rector-Brooks et al., 2024; Wang et al., 2025). Our method leaves the pretrained model fixed, and therefore doesn’t require a costly fine-tuning stage. We note that our method is compatible with a model obtained from reward fine-tuning, or from any training approach resulting in a parameterized rate matrix (Le-Tuyet-Nhi et al., 2025).

Inference Time Alignment. Several methods perform additional computation at inference time to sample from a target product distribution (the product being taken with either an external model $r(x)$, or a classifier extracted from the model’s distribution, $q_t(y|x)$ as in classifier-free guidance (Ho & Salimans, 2022)). These methods often involve an approximation which means they produce biased samples from the target product (Vignac et al., 2022; Gruver et al., 2023; Nisonoff et al., 2024; Tang et al., 2025). Singhal et al. (2025) investigates the use of SMC to sample (in an asymptotically unbiased manner) from a reward-weighted distribution. Our work adapts such an unbiased SMC based strategy to a smoothly annealed form of the reward ($\beta_t r(x)$), and extends it to general products,

and annealing. [He et al. \(2025\)](#) recently proposed another SMC-based technique for such problems, however, they do not evaluate the method on discrete diffusion tasks.

Boltzmann distribution annealing. Our approach for annealing is related to recent works which explore methods to train discrete neural samplers for combinatorial optimization and statistical physics. These include works such as scalable discrete diffusion samplers ([Sanokowski et al., 2025](#)), LEAPS ([Holderrieth et al., 2025](#)), and discrete neural flow samplers with locally equivariant transformers ([Ou et al., 2025](#)). These methods are typically trained to approximate Boltzmann distributions at a range of temperatures (or rely on access to the energy function during training), whereas our method assumes access to a trained model (perhaps with samples from a single temperature) and then uses it to generate samples at different, unseen temperatures through a modified inference algorithm.

Theoretical guarantees. Establishing the convergence bounds on the distribution of the produced samples is a direction of independent interest. In this work, we provide the proof of the Feynman-Kac formula (Theorem 2.1), which establishes the convergence of the time-discretization scheme. However, the community has developed a range of theoretical tools ([Benton et al., 2023](#); [Ren et al., 2024](#); [Le-Tuyet-Nhi et al., 2025](#)) potentially allowing for a more accurate convergence analysis.

6 CONCLUSION

In this paper, we propose DISCRETE FEYNMAN-KAC CORRECTORS, a framework that allows for re-purposing discrete diffusion models at inference time without retraining them. In particular, our theoretical findings demonstrate that sampling from the annealed, product or reward-weighted distributions can be efficiently done by combining the learned probability ratios and running SMC algorithms. Our empirical study supports our derivations and demonstrates that the proposed approach is more effective for tasks such as sampling from lower temperature Ising models, using language models to solve programming problems or inferring parameters, and controlling generated protein sequences. For future work we leave the extension to joint continuous and discrete models, as well as procedures to combine the method with reward fine-tuning.

REPRODUCIBILITY STATEMENT

To facilitate reproducibility of our empirical results and algorithm, we have made our code publicly available at this link: https://github.com/hasanmohsin/discrete_fkc. We describe all mathematical and algorithmic details necessary to reproduce our results throughout this paper (e.g. Alg. 1).

ACKNOWLEDGEMENTS

The research was enabled in part by computational resources provided by the Digital Research Alliance of Canada (<https://alliancecan.ca>), Mila (<https://mila.quebec>), and NVIDIA. This project was partially sponsored by Google through the Google & Mila projects program. KN was supported by IVADO and Institut Courtois. MS was supported by the IVADO 2025 Postdoctoral Research Funding Program. This project was undertaken thanks to funding from IVADO and the Canada First Research Excellence Fund.

REFERENCES

Josh Abramson, Jonas Adler, Jack Dunger, Richard Evans, Tim Green, Alexander Pritzel, Olaf Ronneberger, Lindsay Willmore, Andrew J Ballard, Joshua Bambrick, et al. Accurate structure prediction of biomolecular interactions with alphafold 3. *Nature*, 630(8016):493–500, 2024.

Tara Akhoud-Sadegh, Jungyoon Lee, Avishek Joey Bose, Valentin De Bortoli, Arnaud Doucet, Michael M. Bronstein, Dominique Beaini, Siamak Ravanbakhsh, Kirill Neklyudov, and Alexander Tong. Progressive inference-time annealing of diffusion models for sampling from boltzmann densities. *arXiv preprint arXiv:2506.16471*, 2025.

Sarah Alamdari, Nitya Thakkar, Rianne van den Berg, Neil Tenenholz, Bob Strome, Alan Moses, Alex Xijie Lu, Nicolo Fusi, Ava Pardis Amini, and Kevin K Yang. Protein generation with evolutionary diffusion: sequence is all you need. *BioRxiv*, pp. 2023–09, 2023.

Jacob Austin, Augustus Odena, Maxwell Nye, Maarten Bosma, Henryk Michalewski, David Dohan, Ellen Jiang, Carrie Cai, Michael Terry, Quoc Le, and Charles Sutton. Program synthesis with large language models. *arXiv preprint arXiv:2108.07732*, 2021.

Joe Benton, Valentin De Bortoli, Arnaud Doucet, and George Deligiannidis. Nearly d -linear convergence bounds for diffusion models via stochastic localization. *arXiv preprint arXiv:2308.03686*, 2023.

Joe Benton, Yuyang Shi, Valentin De Bortoli, George Deligiannidis, and Arnaud Doucet. From denoising diffusions to denoising markov models. *Journal of the Royal Statistical Society Series B: Statistical Methodology*, 86(2):286–301, 2024.

Lukas Berglund, Meg Tong, Max Kaufmann, Mikita Balesni, Asa Cooper Stickland, Tomasz Korbak, and Owain Evans. The reversal curse: Llms trained on "a is b" fail to learn "b is a". *arXiv preprint arXiv:2309.12288*, 2023.

Andreas Blattmann, Robin Rombach, Huan Ling, Tim Dockhorn, Seung Wook Kim, Sanja Fidler, and Karsten Kreis. Align your latents: High-resolution video synthesis with latent diffusion models. *Conference on Computer Vision and Pattern Recognition (CVPR)*, 2023.

Tom Brown, Benjamin Mann, Nick Ryder, Melanie Subbiah, Jared D Kaplan, Prafulla Dhariwal, Arvind Neelakantan, Pranav Shyam, Girish Sastry, Amanda Askell, et al. Language models are few-shot learners. *Advances in Neural Information Processing Systems (NeurIPS)*, 33:1877–1901, 2020.

Andrew Campbell, Joe Benton, Valentin De Bortoli, Thomas Rainforth, George Deligiannidis, and Arnaud Doucet. A continuous time framework for discrete denoising models. *Advances in Neural Information Processing Systems (NeurIPS)*, 35:28266–28279, 2022.

Mark Chen, Jerry Tworek, Heewoo Jun, Qiming Yuan, Henrique Ponde de Oliveira Pinto, Jared Kaplan, Harri Edwards, Yuri Burda, Nicholas Joseph, Greg Brockman, Alex Ray, Raul Puri, Gretchen Krueger, Michael Petrov, Heidy Khlaaf, Girish Sastry, Pamela Mishkin, Brooke Chan, Scott Gray, Nick Ryder, Mikhail Pavlov, Alethea Power, Lukasz Kaiser, Mohammad Bavarian, Clemens Winter, Philippe Tillet, Felipe Petroski Such, Dave Cummings, Matthias Plappert, Fotios Chantzis, Elizabeth Barnes, Ariel Herbert-Voss, William Hebgen Guss, Alex Nichol, Alex Paino, Nikolas Tezak, Jie Tang, Igor Babuschkin, Suchir Balaji, Shantanu Jain, William Saunders, Christopher Hesse, Andrew N. Carr, Jan Leike, Josh Achiam, Vedant Misra, Evan Morikawa, Alec Radford, Matthew Knight, Miles Brundage, Mira Murati, Katie Mayer, Peter Welinder, Bob McGrew, Dario Amodei, Sam McCandlish, Ilya Sutskever, and Wojciech Zaremba. Evaluating large language models trained on code. *arXiv 2107.03374*, 2021.

DeepSeek-AI. Deepseek-r1: Incentivizing reasoning capability in llms via reinforcement learning. *arXiv preprint arXiv:2501.12948*, 2025.

Patrick Emami, Aidan Perreault, Jeffrey Law, David Biagioni, and Peter St John. Plug & play directed evolution of proteins with gradient-based discrete mcmc. *Machine Learning: Science and Technology*, 4(2):025014, 2023.

Moritz Ertelt, Jens Meiler, and Clara T Schoeder. Combining rosetta sequence design with protein language model predictions using evolutionary scale modeling (esm) as restraint. *ACS synthetic biology*, 13(4):1085–1092, 2024.

Cade W Gordon, Amy X. Lu, and Pieter Abbeel. Protein language model fitness is a matter of preference. *International Conference on Learning Representations (ICLR)*, 2025. URL <https://openreview.net/forum?id=UvPdpa4LuV>.

Nate Gruver, Samuel Stanton, Nathan Frey, Tim GJ Rudner, Isidro Hotzel, Julien Lafrance-Vanassee, Arvind Rajpal, Kyunghyun Cho, and Andrew G Wilson. Protein design with guided discrete diffusion. *Advances in Neural Information Processing Systems (NeurIPS)*, 36:12489–12517, 2023.

Jiajun He, José Miguel Hernández-Lobato, Yuanqi Du, and Francisco Vargas. Rne: a plug-and-play framework for diffusion density estimation and inference-time control. *arXiv preprint arXiv:2506.05668*, 2025.

Geoffrey E Hinton. Products of experts. *International Conference on Artificial Neural Networks (ICANN)*, 1:1–6, 1999.

Jonathan Ho and Tim Salimans. Classifier-free diffusion guidance. *Advances in Neural Information Processing Systems (NeurIPS) Workshop on Deep Generative Models and Downstream Applications*, 2022. URL <https://arxiv.org/abs/2207.12598>.

Peter Holderrieth, Michael Samuel Albergo, and Tommi Jaakkola. LEAPS: A discrete neural sampler via locally equivariant networks. *International Conference on Machine Learning (ICML)*, 2025.

Audrey Huang, Adam Block, Dylan J. Foster, Dhruv Rohatgi, Cyril Zhang, Max Simchowitz, Jordan T. Ash, and Akshay Krishnamurthy. Self-improvement in language models: The sharpening mechanism. *arXiv preprint arXiv:2412.01951*, 2024.

Andrei Kolmogoroff. Über die analytischen methoden in der wahrscheinlichkeitsrechnung. *Mathematische Annalen*, 104:415–458, 1931.

Pham Le-Tuyet-Nhi, Dario Shariatian, Antonio Ocello, Giovanni Conforti, and Alain Oliviero Durmus. Discrete markov probabilistic models: An improved discrete score-based framework with sharp convergence bounds under minimal assumptions. *International Conference on Machine Learning (ICML)*, 2025.

Seul Lee, Karsten Kreis, Srimukh Prasad Veccham, Meng Liu, Danny Reidenbach, Yuxing Peng, Saeed Paliwal, Weili Nie, and Arash Vahdat. Genmol: A drug discovery generalist with discrete diffusion. *arXiv preprint arXiv:2501.06158*, 2025.

Zeming Lin, Halil Akin, Roshan Rao, Brian Hie, Zhongkai Zhu, Wenting Lu, Nikita Smetanin, Allan dos Santos Costa, Maryam Fazel-Zarandi, Tom Sercu, Sal Candido, et al. Language models of protein sequences at the scale of evolution enable accurate structure prediction. *bioRxiv*, 2022.

Zeming Lin, Halil Akin, Roshan Rao, Brian Hie, Zhongkai Zhu, Wenting Lu, Nikita Smetanin, Robert Verkuil, Ori Kabeli, Yaniv Shmueli, Allan dos Santos Costa, Maryam Fazel-Zarandi, Tom Sercu, Salvatore Candido, and Alexander Rives. Evolutionary-scale prediction of atomic-level protein structure with a language model. *Science*, 379(6637):1123–1130, 2023. doi: 10.1126/science.ade2574. URL <https://www.science.org/doi/abs/10.1126/science.ade2574>.

Aaron Lou, Chenlin Meng, and Stefano Ermon. Discrete diffusion language modeling by estimating the ratios of the data distribution. *International Conference on Machine Learning (ICML)*, 2024.

Ali Madani, Ben Krause, Eric R. Greene, Subu Subramanian, Benjamin P. Mohr, James M. Holton, Jose Luis Olmos, Caiming Xiong, Zachary Z. Sun, Richard Socher, James S. Fraser, and Nikhil Naik. Large language models generate functional protein sequences across diverse families. *Nature Biotechnology*, 41(8):1099–1106, Aug 2023. ISSN 1546-1696. doi: 10.1038/s41587-022-01618-2. URL <https://doi.org/10.1038/s41587-022-01618-2>.

Sarthak Mittal, Niels Leif Bracher, Guillaume Lajoie, Priyank Jaini, and Marcus Brubaker. Amortized in-context bayesian posterior estimation. *arXiv preprint arXiv:2502.06601*, 2025. URL <https://arxiv.org/abs/2502.06601>.

Shen Nie, Fengqi Zhu, Zebin You, Xiaolu Zhang, Jingyang Ou, Jun Hu, Jun Zhou, Yankai Lin, Ji-Rong Wen, and Chongxuan Li. Large language diffusion models. *arXiv preprint arXiv:2502.09992*, 2025. URL <https://arxiv.org/abs/2502.09992>.

Hunter Nisonoff, Junhao Xiong, Stephan Allenspach, and Jennifer Listgarten. Unlocking guidance for discrete state-space diffusion and flow models. *arXiv preprint arXiv:2406.01572*, 2024.

Pascal Notin, Aaron Kollasch, Daniel Ritter, Lood van Niekerk, Steffanie Paul, Han Spinner, Nathan Rollins, Ada Shaw, Rose Orenbuch, Ruben Weitzman, Jonathan Frazer, Mafalda Dias, Dinko Franceschi, Yarin Gal, and Debora Marks. Proteingym: Large-scale benchmarks for protein fitness prediction and design. *Advances in Neural Information Processing Systems (NeurIPS)*, 2023.

Zijing Ou, Ruixiang Zhang, and Yingzhen Li. Discrete neural flow samplers with locally equivariant transformer. *arXiv preprint arXiv:2505.17741*, 2025.

Jarrid Rector-Brooks, Mohsin Hasan, Zhangzhi Peng, Zachary Quinn, Chenghao Liu, Sarthak Mittal, Nouha Dziri, Michael Bronstein, Yoshua Bengio, Pranam Chatterjee, et al. Steering masked discrete diffusion models via discrete denoising posterior prediction. *arXiv preprint arXiv:2410.08134*, 2024.

Yinuo Ren, Haoxuan Chen, Grant M Rotskoff, and Lexing Ying. How discrete and continuous diffusion meet: Comprehensive analysis of discrete diffusion models via a stochastic integral framework. *arXiv preprint arXiv:2410.03601*, 2024.

James Requeima, John F Bronskill, Dami Choi, Richard E. Turner, and David Duvenaud. LLM processes: Numerical predictive distributions conditioned on natural language. *Advances in Neural Information Processing Systems (NeurIPS)*, 2024. URL <https://openreview.net/forum?id=HShs7q1Njh>.

Robin Rombach, Andreas Blattmann, Dominik Lorenz, Patrick Esser, and Björn Ommer. High-resolution image synthesis with latent diffusion models. *Conference on Computer Vision and Pattern Recognition (CVPR)*, 2022.

Chitwan Saharia, William Chan, Saurabh Saxena, Lala Li, Jay Whang, Emily L Denton, Kamyar Ghasemipour, Raphael Gontijo Lopes, Burcu Karagol Ayan, Tim Salimans, et al. Photorealistic text-to-image diffusion models with deep language understanding. *Advances in Neural Information Processing Systems (NeurIPS)*, 35:36479–36494, 2022.

Subham Sekhar Sahoo, Marianne Arriola, Yair Schiff, Aaron Gokaslan, Edgar Marroquin, Justin T Chiu, Alexander Rush, and Volodymyr Kuleshov. Simple and effective masked diffusion language models. *arXiv preprint arXiv:2406.07524*, 2024.

Sebastian Sanokowski, Wilhelm Berghammer, Martin Ennemoser, Haoyu Peter Wang, Sepp Hochreiter, and Sebastian Lehner. Scalable discrete diffusion samplers: Combinatorial optimization and statistical physics. *arXiv preprint arXiv:2502.08696*, 2025.

Jiaxin Shi, Kehang Han, Zhe Wang, Arnaud Doucet, and Michalis K Titsias. Simplified and generalized masked diffusion for discrete data. *arXiv preprint arXiv:2406.04329*, 2024.

Raghav Singhal, Zachary Horvitz, Ryan Teehan, Mengye Ren, Zhou Yu, Kathleen McKeown, and Rajesh Ranganath. A general framework for inference-time scaling and steering of diffusion models. *International Conference on Machine Learning (ICML)*, 2025.

Marta Skreta, Lazar Atanackovic, Joey Bose, Alexander Tong, and Kirill Neklyudov. The superposition of diffusion models using the itô density estimator. *International Conference on Learning Representations (ICLR)*, 2024.

Marta Skreta, Tara Akhoud-Sadegh, Viktor Ohanesian, Roberto Bondesan, Alán Aspuru-Guzik, Arnaud Doucet, Rob Brekelmans, Alexander Tong, and Kirill Neklyudov. Feynman-kac correctors in diffusion: Annealing, guidance, and product of experts. *arXiv preprint arXiv:2503.02819*, 2025.

Yang Song, Jascha Sohl-Dickstein, Diederik P. Kingma, Abhishek Kumar, Stefano Ermon, and Ben Poole. Score-based generative modeling through stochastic differential equations. *arXiv preprint arXiv:2011.13456*, 2021.

Martin Steinegger and Johannes Söding. Mmseqs2 enables sensitive protein sequence searching for the analysis of massive data sets. *Nature biotechnology*, 35(11):1026–1028, 2017.

Robert H Swendsen and Jian-Sheng Wang. Nonuniversal critical dynamics in monte carlo simulations. *Physical review letters*, 58(2):86, 1987.

Sophia Tang, Yinuo Zhang, and Pranam Chatterjee. Peptune: De novo generation of therapeutic peptides with multi-objective-guided discrete diffusion. *arXiv preprint arXiv:2412.17780*, 2025.

Michel van Kempen, Stephanie S Kim, Charlotte Tumescheit, Milot Mirdita, Johannes Söding, and Martin Steinegger. Fast and accurate protein structure search with foldseek. *Nature Biotechnology*, 42, 2024. doi: 10.1038/s41587-023-01773-0.

Siddarth Venkatraman, Moksh Jain, Luca Scimeca, Minsu Kim, Marcin Sendera, Mohsin Hasan, Luke Rowe, Sarthak Mittal, Pablo Lemos, Emmanuel Bengio, Alexandre Adam, Jarrid Rector-Brooks, Yoshua Bengio, Glen Berseth, and Nikolay Malkin. Amortizing intractable inference in diffusion models for vision, language, and control. *Advances in Neural Information Processing Systems (NeurIPS)*, 2024. URL <https://openreview.net/forum?id=gVTkMsaaGI>.

Clement Vignac, Igor Krawczuk, Antoine Siraudin, Bohan Wang, Volkan Cevher, and Pascal Frossard. Digress: Discrete denoising diffusion for graph generation. *arXiv preprint arXiv:2209.14734*, 2022.

Pierre-A Vuillermot. A generalization of chernoff's product formula for time-dependent operators. *Journal of Functional Analysis*, 259(11):2923–2938, 2010.

Chenyu Wang, Masatoshi Uehara, Yichun He, Amy Wang, Avantika Lal, Tommi Jaakkola, Sergey Levine, Aviv Regev, Hanchen, and Tommaso Biancalani. Fine-tuning discrete diffusion models via reward optimization with applications to DNA and protein design. *International Conference on Learning Representations (ICLR)*, 2025.

Jiuniu Wang, Hangjie Yuan, Dayou Chen, Yingya Zhang, Xiang Wang, and Shiwei Zhang. Mod-elscope text-to-video technical report. *arXiv preprint arXiv:2308.06571*, 2023.

Xinyou Wang, Zaixiang Zheng, Fei Ye, Dongyu Xue, Shujian Huang, and Quanquan Gu. Diffusion language models are versatile protein learners. *arXiv preprint arXiv:2402.18567*, 2024a.

Xinyou Wang, Zaixiang Zheng, Fei Ye, Dongyu Xue, Shujian Huang, and Quanquan Gu. Diffusion language models are versatile protein learners. *International Conference on Machine Learning (ICML)*, 2024b.

Joseph L Watson, David Juergens, Nathaniel R Bennett, Brian L Trippe, Jason Yim, Helen E Eisenach, Woody Ahern, Andrew J Borst, Robert J Ragotte, Lukas F Milles, et al. De novo design of protein structure and function with rfdiffusion. *Nature*, 620(7976):1089–1100, 2023.

Jinrui Xu and Yang Zhang. How significant is a protein structure similarity with tm-score= 0.5? *Bioinformatics*, 26(7):889–895, 2010.

An Yang, Baosong Yang, Binyuan Hui, Bo Zheng, Bowen Yu, Chang Zhou, Chengpeng Li, Chengyuan Li, Dayiheng Liu, Fei Huang, Guanting Dong, Haoran Wei, Huan Lin, Jialong Tang, Jialin Wang, Jian Yang, Jianhong Tu, Jianwei Zhang, Jianxin Ma, Jin Xu, Jingren Zhou, Jinze Bai, Jinzheng He, Junyang Lin, Kai Dang, Keming Lu, Keqin Chen, Kexin Yang, Mei Li, Mingfeng Xue, Na Ni, Pei Zhang, Peng Wang, Ru Peng, Rui Men, Ruize Gao, Runji Lin, Shijie Wang, Shuai Bai, Sinan Tan, Tianhang Zhu, Tianhao Li, Tianyu Liu, Wenbin Ge, Xiaodong Deng, Xiaohuan Zhou, Xingzhang Ren, Xinyu Zhang, Xipin Wei, Xuancheng Ren, Yang Fan, Yang Yao, Yichang Zhang, Yu Wan, Yunfei Chu, Yuqiong Liu, Zeyu Cui, Zhenru Zhang, and Zhihao Fan. Qwen2 technical report. *arXiv preprint arXiv:2407.10671*, 2024.

Yang Zhang and Jeffrey Skolnick. Scoring function for automated assessment of protein structure template quality. *Proteins: Structure*, 57, 2004.

A METHOD OVERVIEW

A.1 CORRESPONDENCE TO CONTINUOUS FEYNMAN-KAC CORRECTORS

Table A1: Comparison of state updates for DISCRETE FEYNMAN-KAC CORRECTORS and continuous Feynman-Kac Correctors (Skreta et al., 2025), corresponding to line 4 in Alg. 1. For computing $r_{l,j}^{\text{diff}}$ in the case of sampling from the reward-tilted distribution, $x_t^{l,j}$ is x_t , except that position l is replaced with token j , where l is the position being de-masked and j is a token from the vocabulary.

	Target	DFKC	FKC
Base	$p_t(x)$	$x_{t+\Delta t} \sim \text{softmax}(\text{NN}(x_t))$	$x_{t+\Delta t} = x_t + (-f_t(x_t) + \sigma_t^2 \text{NN}(x_t))\Delta t + \sigma_t \Delta W_t$
Annealing	$p_t^\beta(x)$	$x_{t+\Delta t} \sim \text{softmax}(\beta \text{NN}(x_t))$	$x_{t+\Delta t} = x_t + (-f_t(x_t) + \beta \sigma_t^2 \text{NN}(x_t))\Delta t + \sigma_t \Delta W_t$
Product	$p_t^1(x)p_t^2(x)$	$x_{t+\Delta t} \sim \text{softmax}(\text{NN}^1(x_t) + \text{NN}^2(x_t))$	$x_{t+\Delta t} = x_t + (-f_t(x_t) + \sigma_t^2 (\text{NN}^1(x_t) + \text{NN}^2(x_t)))\Delta t + \sigma_t \Delta W_t$
Reward	$p_t(x) \exp(\beta_t r(x))$	$[1] r_{l,j}^{\text{diff}} = \beta_t(r(x_t^{l,j}) - r(x_t))$ $[2] x_{t+\Delta t} \sim \text{softmax}(\text{NN}(x_t) + r^{\text{diff}})$	$x_{t+\Delta t} = x_t + (-f_t(x_t) + \sigma_t^2 \text{NN}(x_t) + \beta_t \frac{\sigma_t^2}{2} \nabla r(x_t))\Delta t + \sigma_t \Delta W_t$

Table A2: Comparison of weight updates for DISCRETE FEYNMAN-KAC CORRECTORS and continuous Feynman-Kac Correctors (Skreta et al., 2025), corresponding to line 5 in Alg. 1.

	Target	DFKC	FKC
Base	$p_t(x)$	—	—
Annealing	$p_t^\beta(x)$	$g_t(x_t) = \beta \frac{(1-t)^{\beta-1}}{t^\beta} \sum_j \text{softmax}(\beta \text{NN}(x_t)_j)$	$g_t(x_t) = (\beta - 1)(\langle \nabla, f_t(x_t) \rangle + \frac{\sigma_t^2}{2} \beta \ \text{NN}(x_t)\ ^2 \Delta t)$
Product	$p_t^1(x)p_t^2(x)$	$g_t(x_t) = 2 \frac{(1-t)}{t^2} \sum_j \text{softmax}(\text{NN}^1(x_t)_j + \text{NN}^2(x_t)_j)$	$g_t(x_t) = (\langle \nabla, f_t(x_t) \rangle + \sigma_t^2 \langle \text{NN}^1(x_t), \text{NN}^2(x_t) \rangle) \Delta t$
Reward	$p_t(x) \exp(\beta_t r(x))$	$g_t(x_t) = \frac{1}{t} \sum_j \text{softmax}(\text{NN}(x_t)_j + r^{\text{diff}}) + \Delta \beta_t r(x_t)$	$g_t(x_t) = (\langle \beta_t \nabla r(x_t), \frac{\sigma_t^2}{2} \text{NN}(x_t) - f_t(x_t) \rangle + \Delta \beta_t r(x_t)) \Delta t$

B BACKGROUND PROOFS

B.1 WEIGHTED FORWARD KOLMOGOROV EQUATION

Consider the forward Kolmogorov equation with the weighting term

$$\frac{\partial p_s(j)}{\partial s} = \sum_{k \neq j} A_s(k, j)p_s(k) - \sum_{k \neq j} A_s(j, k)p_s(j) + p_s(j)(g_s(j) - \sum_k p_s(k)g_s(k)). \quad (22)$$

We can re-write the last term as

$$p_s(j)(g_s(j) - \sum_k p_s(k)g_s(k)) = \sum_k p_s(k)p_s(j)(g_s(j) - g_s(k)) \quad (23)$$

$$= \sum_k p_s(k)p_s(j)\sigma_s(j, k)|g_s(j) - g_s(k)| \quad (24)$$

$$= \sum_k p_s(j)\mathbb{1}[\sigma_s(j, k) > 0]|g_s(j) - g_s(k)|p_s(k) - \quad (25)$$

$$- \sum_k p_s(k)\mathbb{1}[\sigma_s(j, k) < 0]|g_s(j) - g_s(k)|p_s(j), \quad (26)$$

where $\sigma_s(j, k)$ is the sign of $(g_s(j) - g_s(k))$. Let's define

$$B_s(k, j) := p_s(k)\mathbb{1}[\sigma_s(j, k) > 0]|g_s(j) - g_s(k)| \quad (27)$$

$$\implies B_s(j, k) := p_s(j)\mathbb{1}[\sigma_s(k, j) > 0]|g_s(k) - g_s(j)|. \quad (28)$$

Using the fact that $\sigma_s(k, j) = -\sigma_s(j, k)$, we have

$$p_s(j)(g_s(j) - \sum_k p_s(k)g_s(k)) = \sum_k B_s(k, j)p_s(k) - \sum_k B_s(j, k)p_s(j). \quad (29)$$

Finally, using the fact that $B_s(j, j) = 0$, we have

$$\frac{\partial p_s(j)}{\partial s} = \sum_{k \neq j} A_s(k, j)p_s(k) - \sum_{k \neq j} A_s(j, k)p_s(j) + p_s(j)(g_s(j) - \sum_k p_s(k)g_s(k)) \quad (30)$$

$$= \sum_{k \neq j} (A_s(k, j) + B_s(k, j))p_s(k) - \sum_{k \neq j} (A_s(j, k) + B_s(j, k))p_s(j), \quad (31)$$

$$B_s(k, j) := p_s(k)\mathbb{1}[\sigma_s(j, k) > 0]|g_s(j) - g_s(k)|. \quad (32)$$

B.2 DISCRETE FEYNMAN-KAC FORMULA

Theorem 2.1. [Feynman-Kac Formula] *For the forward Kolmogorov equation from Equation (4) describing the time-evolution of the marginals $p_t(i)$ with the rate matrix $A_t(i, j)$ and weights $g_t(i)$, $\bar{g}_t(i) = g_t(i) - \sum_k p_t(k)g_t(k)$*

$$\begin{aligned} \mathbb{E}_{p_T(x)}\phi(x) &= \lim_{dt \rightarrow 0} \sum_{x_T} \dots \sum_{x_0} \phi(x_T)p(x_T | x_{T-dt}) \dots p(x_{dt} | x_0) \exp\left(\sum_{t=0}^T dt \bar{g}_t(x_t)\right) p_0(x_0) \\ &= \mathbb{E}_{X_{0:T}} \exp\left(\int_0^T dt \bar{g}_t(X_t)\right) \phi(X_T) \propto \mathbb{E}_{X_{0:T}} \exp\left(\int_0^T dt g_t(X_t)\right) \phi(X_T), \end{aligned} \quad (5)$$

where the expectation on the right hand side is taken w.r.t. trajectories $X_{0:T}$ defined as the limit of the transitions from Equation (3).

Proof. We re-write the following FKE in the matrix notation, i.e.

$$\frac{\partial p_t(i)}{\partial t} = \sum_{j \neq i} A_t(j, i)p_t(j) - \sum_{j \neq i} A_t(i, j)p_t(i) + p_t(i)(g_t(i) - \sum_k p_t(k)g_t(k)) \quad (33)$$

$$= \sum_j A_t(j, i)p_t(j) + \sum_j \delta_{ij}\bar{g}_t(i)p_t(j) \quad (34)$$

$$= [\mathbf{A}_t \mathbf{p}_t]_i + [\mathbf{G}_t \mathbf{p}_t]_i, \quad (35)$$

where we define the matrices \mathbf{A}_t and \mathbf{G}_t as

$$[\mathbf{A}_t]_{ij} := A_t(j, i), \quad [\mathbf{G}_t]_{ij} := \delta_{ij}\bar{g}_t(i), \quad \bar{g}_t(i) = g_t(i) - \sum_k p_t(k)g_t(k). \quad (36)$$

Thus, in the matrix notation, we have the following Ordinary Differential Equation (ODE)

$$\frac{\partial \mathbf{p}_t}{\partial t} = (\mathbf{A}_t + \mathbf{G}_t)\mathbf{p}_t, \quad (37)$$

which solution is given by the time-ordered exponential, denoted as

$$\mathbf{p}_T = \mathcal{T} \exp\left(\int_0^T dt (\mathbf{A}_t + \mathbf{G}_t)\right) \mathbf{p}_0, \quad (38)$$

and defined as the following limit

$$\mathbf{p}_T = \lim_{n \rightarrow \infty} \prod_{k=0}^{n-1} \exp\left(\frac{1}{n}(\mathbf{A}_{(kT)/n} + \mathbf{G}_{(kT)/n})\right) \mathbf{p}_0. \quad (39)$$

Using the time-dependent analog of the Lie-Trotter formula (see (Vuillermot, 2010) for the proof), we can re-write the matrix exponential of the sum as the product of matrix exponentials, which is not true in general because \mathbf{A}_t and \mathbf{G}_t do not commute i.e.

$$\lim_{n \rightarrow \infty} \prod_{k=0}^{n-1} \exp\left(\frac{1}{n}(\mathbf{A}_{(kT)/n} + \mathbf{G}_{(kT)/n})\right) = \lim_{n \rightarrow \infty} \prod_{k=0}^{n-1} \exp\left(\frac{1}{n}\mathbf{A}_{(kT)/n}\right) \exp\left(\frac{1}{n}\mathbf{G}_{(kT)/n}\right).$$

Denoting $dt := 1/n$ and $t_k = (kT)/n$, we have

$$\mathbf{p}_T = \lim_{dt \rightarrow 0} \prod_{k=0}^{n-1} \exp(dt \mathbf{A}_{t_k}) \exp(dt \mathbf{G}_{t_k}) \mathbf{p}_0 \quad (40)$$

$$= \lim_{dt \rightarrow 0} \prod_{k=1}^{n-1} \exp(dt \mathbf{A}_{t_k}) \exp(dt \mathbf{G}_{t_k}) \sum_{j_0} \exp(dt \mathbf{A}_{t_0})_{i_1 j_0} \sum_{i_0} \exp(dt \mathbf{G}_{t_0})_{j_0 i_0} p_0(i_0). \quad (41)$$

Using the fact that \mathbf{G}_t is diagonal, we have

$$\exp(dt \mathbf{G}_t)_{ij} = \delta_{ij} \exp(dt \bar{g}_t(i)), \quad (42)$$

and, correspondingly,

$$p_T(i) = \lim_{dt \rightarrow 0} \prod_{k=1}^{n-1} \exp(dt \mathbf{A}_{t_k}) \exp(dt \mathbf{G}_{t_k}) \sum_{j_0} \sum_{i_0} \exp(dt \mathbf{A}_{t_0})_{i_1 j_0} \delta_{j_0 i_0} \exp(dt \bar{g}_{t_0}(j_0)) p_0(i_0) \quad (43)$$

$$= \lim_{dt \rightarrow 0} \prod_{k=1}^{n-1} \exp(dt \mathbf{A}_{t_k}) \exp(dt \mathbf{G}_{t_k}) \sum_{i_0} \exp(dt \mathbf{A}_{t_0})_{i_1 i_0} \exp(dt \bar{g}_{t_0}(i_0)) p_0(i_0) \quad (44)$$

$$= \lim_{dt \rightarrow 0} \sum_{i_{n-2}} \dots \sum_{i_1} \sum_{i_0} \exp(dt \mathbf{A}_{t_{n-1}})_{i_1 i_{n-2}} \exp(dt \bar{g}_{t_{n-2}}(i_{n-2})) \dots \quad (45)$$

$$\cdot \exp(dt \mathbf{A}_{t_0})_{i_1 i_0} \exp(dt \bar{g}_{t_0}(i_0)) p_0(i_0) \quad (46)$$

$$= \lim_{dt \rightarrow 0} \sum_{i_{n-2}} \dots \sum_{i_0} \exp(dt \mathbf{A}_{t_{n-1}})_{i_1 i_{n-2}} \dots \exp(dt \mathbf{A}_{t_0})_{i_1 i_0} \exp\left(\sum_{k=0}^{n-2} dt \bar{g}_{t_k}(i_k)\right) p_0(i_0).$$

Finally, we denote

$$p(x_{t+dt} = i \mid x_t = j) := \exp(dt \mathbf{A}_t)_{ij} = \delta_{ij} + A_t(j, i)dt + o(dt). \quad (47)$$

In this notation, the expected value of the statistics ϕ can be evaluated as

$$\begin{aligned} \sum_x \phi(x) p_T(x) &= \lim_{dt \rightarrow 0} \sum_{x_T} \dots \sum_{x_0} \phi(x_T) p(x_T \mid x_{T-dt}) \dots p(x_{dt} \mid x_0) \exp\left(\sum_{t=0}^T dt \bar{g}_t(x_t)\right) p_0(x_0) \\ &= \mathbb{E}_{X_{0:T}} \exp\left(\int_0^T dt \bar{g}_t(X_t)\right) \phi(X_T) \propto \mathbb{E}_{X_{0:T}} \exp\left(\int_0^T dt g_t(X_t)\right) \phi(X_T), \end{aligned} \quad (48)$$

where in the last two formulas we take the expectation w.r.t. the process $X_{0:T}$ defined as the limit of the transition distributions $p(x_{t+dt} = i \mid x_t = j)$. \square

B.3 DISCRETE MASKED DIFFUSION

First, we consider general case, where m is the mask state and $\alpha_{s,t}$ is the noise schedule, i.e. the noising process is defined as

$$p(x_s = j \mid x_t = i) = (1 - \bar{\alpha}_{s,t})\delta_{mj} + \bar{\alpha}_{s,t}\delta_{ij}. \quad (49)$$

Note that not every $\bar{\alpha}_{s,t}$ satisfies the master equation and we have to ensure that the following equality holds.

$$p(x_s = j \mid x_t = i) = \sum_k p(x_s = j \mid x_r = k) p(x_r = k \mid x_t = i) \quad (50)$$

$$(1 - \bar{\alpha}_{s,t})\delta_{mj} + \bar{\alpha}_{s,t}\delta_{ij} = \sum_k ((1 - \bar{\alpha}_{s,r})\delta_{mj} + \bar{\alpha}_{s,r}\delta_{kj})((1 - \bar{\alpha}_{r,t})\delta_{mk} + \bar{\alpha}_{r,t}\delta_{ik}) \quad (51)$$

$$\begin{aligned} (1 - \bar{\alpha}_{s,t})\delta_{mj} + \bar{\alpha}_{s,t}\delta_{ij} &= (1 - \bar{\alpha}_{s,r})\delta_{mj}(\bar{\alpha}_{r,t} + (1 - \bar{\alpha}_{r,t})) + \bar{\alpha}_{s,r}((1 - \bar{\alpha}_{r,t})\delta_{mj} + \bar{\alpha}_{r,t}\delta_{ij}) \\ (1 - \bar{\alpha}_{s,t})\delta_{mj} + \bar{\alpha}_{s,t}\delta_{ij} &= ((1 - \bar{\alpha}_{s,r}) + \bar{\alpha}_{s,r}(1 - \bar{\alpha}_{r,t}))\delta_{mj} + \bar{\alpha}_{s,r}\bar{\alpha}_{r,t}\delta_{ij}. \end{aligned} \quad (52)$$

Thus, the following relations must hold

$$1 - \bar{\alpha}_{s,t} = (1 - \bar{\alpha}_{s,r}) + \bar{\alpha}_{s,r}(1 - \bar{\alpha}_{r,t}), \quad \bar{\alpha}_{s,t} = \bar{\alpha}_{s,r}\bar{\alpha}_{r,t} \quad (53)$$

$$-\bar{\alpha}_{s,t} = -\bar{\alpha}_{r,t}\bar{\alpha}_{s,r}, \quad \bar{\alpha}_{s,t} = \bar{\alpha}_{s,r}\bar{\alpha}_{r,t}, \quad (54)$$

$$\bar{\alpha}_{s,t} = \bar{\alpha}_{r,t}\bar{\alpha}_{s,r}. \quad (55)$$

Thus, any function that satisfy the following equation works

$$\forall t \leq r \leq s, \quad \bar{\alpha}_{s,t} = \bar{\alpha}_{s,r}\bar{\alpha}_{r,t}. \quad (56)$$

Denoting $\alpha_s = \bar{\alpha}_{s,0}$, we have

$$\bar{\alpha}_{s,t} = \frac{\alpha_s}{\alpha_t}, \text{ and } p(x_s = j | x_t = i) = \left(1 - \frac{\alpha_s}{\alpha_t}\right)\delta_{mj} + \frac{\alpha_s}{\alpha_t}\delta_{ij}. \quad (57)$$

From here, the rate matrix of the noising process is

$$A_t(i, j) = \frac{\partial p(x_s = j | x_t = i)}{\partial s} \Big|_{s=t} = \frac{1}{\alpha_t} \frac{\partial \alpha_t}{\partial t} (\delta_{ij} - \delta_{mj}). \quad (58)$$

B.4 REVERSE-TIME MASKED DIFFUSION

For the inverse time $\tau = 1 - t$, we flip the marginals $q_\tau(i) := p_{1-\tau}(i)$ and take the derivative w.r.t. τ

$$\frac{\partial q_\tau(i)}{\partial \tau} = \frac{\partial p_{1-\tau}(i)}{\partial \tau} = -\frac{\partial p_t(i)}{\partial t} \Big|_{t=1-\tau} \quad (59)$$

$$= -\sum_{j \neq i} (A_{1-\tau}(j, i)p_{1-\tau}(j) - A_{1-\tau}(i, j)p_{1-\tau}(i)) \quad (60)$$

$$= \sum_{j \neq i} \left(A_{1-\tau}(i, j) \frac{p_{1-\tau}(i)}{q_\tau(j)} q_\tau(j) - A_{1-\tau}(j, i) \frac{p_{1-\tau}(j)}{q_\tau(i)} q_\tau(i) \right) \quad (61)$$

$$= \sum_{j \neq i} (B_\tau(j, i)q_\tau(j) - B_\tau(i, j)q_\tau(i)), \quad B_\tau(i, j) := A_{1-\tau}(j, i) \frac{p_{1-\tau}(j)}{p_{1-\tau}(i)}. \quad (62)$$

Note that here we define only the off-diagonal elements and the diagonal elements are

$$B_\tau(i, i) = -\sum_{j \neq i} B_\tau(i, j) = -\sum_{j \neq i} A_{1-\tau}(j, i) \frac{p_{1-\tau}(j)}{p_{1-\tau}(i)}. \quad (63)$$

In particular, for the masked diffusion, we have

$$B_\tau(i, j) = \frac{1}{\alpha_t} \frac{\partial \alpha_t}{\partial t} (\delta_{ij} - \delta_{mi}) \frac{p_t(j)}{p_t(i)}, \quad i \neq j \quad (64)$$

$$= -\frac{1}{\alpha_t} \frac{\partial \alpha_t}{\partial t} \frac{p_t(j)}{p_t(m)} \delta_{mi}, \quad (65)$$

$$B_\tau(i, i) = -\sum_{j \neq i} B_\tau(i, j) = \frac{1}{\alpha_t} \frac{\partial \alpha_t}{\partial t} \frac{1 - p_t(m)}{p_t(m)} \delta_{mi}. \quad (66)$$

B.5 DE-MASKING PARAMETERIZATION

Furthermore, analogously to the derivation from (Shi et al., 2024) (Appendix H.3), we have

$$\frac{p_t(j)}{p_t(m)} = \sum_i \frac{p_0(i)}{p_t(m)} p(x_t = j | x_0 = i) \quad (67)$$

$$= \sum_i \frac{p_0(i)p(x_t = m | x_0 = i)}{p_t(m)p(x_0 = i | x_t = m)} \frac{p(x_0 = i | x_t = m)}{p(x_t = m | x_0 = i)} p(x_t = j | x_0 = i) \quad (68)$$

$$= \sum_i \frac{p(x_0 = i | x_t = m)}{p(x_t = m | x_0 = i)} p(x_t = j | x_0 = i) \quad (69)$$

$$= \sum_i \frac{p(x_0 = i | x_t = m)}{(1 - \alpha_t) + \alpha_t \delta_{im}} ((1 - \alpha_t)\delta_{mj} + \alpha_t \delta_{ij}) \quad (70)$$

$$= \frac{1}{1 - \alpha_t} \sum_i ((1 - \alpha_t)\delta_{mj} + \alpha_t \delta_{ij}) p(x_0 = i | x_t = m) \quad (71)$$

$$= \delta_{mj} + \frac{\alpha_t}{1 - \alpha_t} p(x_0 = j | x_t = m). \quad (72)$$

where we used the fact that $p(x_0 = m) = 0$.

B.6 MULTIDIMENSIONAL CASE

For the multi-dimensional case, we consider the masking process applied independently to each coordinate, i.e.

$$p(x_s = [j_1 \dots j_d] \mid x_t = [i_1 \dots i_d]) = \prod_{k=1}^d p(x_s[k] = j_k \mid x_t[k] = i_k) \quad (73)$$

$$= \prod_{k=1}^d \left(\left(1 - \frac{\alpha_s}{\alpha_t} \right) \delta_{m j_k} + \frac{\alpha_s}{\alpha_t} \delta_{i_k j_k} \right), \quad (74)$$

which defines the following rate matrix

$$A_t([i_1 \dots i_d], [j_1 \dots j_d]) = \frac{\partial p(x_s = [j_1 \dots j_d] \mid x_t = [i_1 \dots i_d])}{\partial s} \Big|_{s=t} \quad (75)$$

$$= \sum_{k=1}^d \prod_{l \neq k} p(x_t[l] = j_l \mid x_t[l] = i_l) \frac{\partial p(x_s[k] = j_k \mid x_t[k] = i_k)}{\partial s} \Big|_{s=t} \quad (76)$$

$$= \frac{1}{\alpha_t} \frac{\partial \alpha_t}{\partial t} \sum_{k=1}^d \prod_{l \neq k} \delta_{j_l i_l} (\delta_{i_k j_k} - \delta_{m j_k}). \quad (77)$$

For the off-diagonal elements of the reverse-time matrix, we have

$$B_t([i_1 \dots i_d], [j_1 \dots j_d]) = A_t([j_1 \dots j_d], [i_1 \dots i_d]) \frac{p_t([j_1 \dots j_d])}{p_t([i_1 \dots i_d])} \quad (78)$$

$$= \frac{1}{\alpha_t} \frac{\partial \alpha_t}{\partial t} \frac{p_t([j_1 \dots j_d])}{p_t([i_1 \dots i_d])} \sum_{k=1}^d \prod_{l \neq k} \delta_{j_l i_l} (\delta_{i_k j_k} - \delta_{m i_k}) \quad (79)$$

$$= - \frac{1}{\alpha_t} \frac{\partial \alpha_t}{\partial t} \frac{p_t([j_1 \dots j_d])}{p_t([i_1 \dots i_d])} \sum_{k=1}^d \prod_{l \neq k} \delta_{j_l i_l} \delta_{m i_k}. \quad (80)$$

C DISCRETE FEYNMAN-KAC CORRECTORS PROOFS

C.1 ANNEALING OF FKE

Theorem 3.1. [Temperature Annealing] Consider the forward Kolmogorov equation from Equation (2) describing the time-evolution of the marginals $p_t(i)$ with the rate matrix $A_t(i, j)$. For the temperature annealed marginals $q_t(i) \propto p_t(i)^\beta$, the following equation holds

$$\frac{\partial q_t(i)}{\partial t} = \sum_{j \neq i} \left(A_t^{\text{anneal}}(j, i) q_t(j) - A_t^{\text{anneal}}(i, j) q_t(i) \right) + q_t(i) (g_t(i) - \mathbb{E}_{q_t(j)} g_t(j)), \quad (12)$$

$$\text{where } A_t^{\text{anneal}}(i, j) := \beta A_t(i, j) \frac{p_t^{1-\beta}(i)}{p_t^{1-\beta}(j)}, \quad g_t(i) := \sum_{j \neq i} (A_t^{\text{anneal}}(i, j) - \beta A_t(i, j)). \quad (13)$$

Proof. Consider the forward Kolmogorov equation for the given rate matrix $A_t(i, j)$

$$\frac{\partial p_t(i)}{\partial t} = \sum_{j \neq i} A_t(j, i) p_t(j) - \sum_{j \neq i} A_t(i, j) p_t(i) \quad (81)$$

$$\frac{\partial}{\partial t} \log p_t(i) = \sum_{j \neq i} A_t(j, i) \frac{p_t(j)}{p_t(i)} - \sum_{j \neq i} A_t(i, j) = \sum_{j \neq i} \left(A_t(j, i) \frac{p_t(j)}{p_t(i)} - A_t(i, j) \right). \quad (82)$$

Then the annealed target $q_t(i) := p_t^\beta(i)/Z_t$ follows

$$\frac{\partial}{\partial t} \log q_t(i) = \beta \frac{\partial}{\partial t} \log p_t(i) - \frac{\partial}{\partial t} \log Z_t \quad (83)$$

$$= \sum_{j \neq i} \left(\beta A_t(j, i) \frac{p_t(j)}{p_t(i)} - \beta A_t(i, j) \right) - \frac{\partial}{\partial t} \log Z_t \quad (84)$$

$$= \sum_{j \neq i} \left(\underbrace{\beta A_t(j, i) \frac{p_t^{1-\beta}(j)}{p_t^{1-\beta}(i)} \frac{q_t(j)}{q_t(i)}}_{:= A_t^{\text{anneal}}(j, i)} - A_t^{\text{anneal}}(i, j) \right) + \quad (85)$$

$$+ \sum_{j \neq i} (A_t^{\text{anneal}}(i, j) - \beta A_t(i, j)) - \frac{\partial}{\partial t} \log Z_t. \quad (86)$$

Denoting the second term as $g_t(j)$, we have

$$\frac{\partial q_t(i)}{\partial t} = \sum_{j \neq i} \left(A_t^{\text{anneal}}(j, i) q_t(j) - A_t^{\text{anneal}}(i, j) q_t(i) \right) + q_t(i) \left(g_t(i) - \frac{\partial}{\partial t} \log Z_t \right), \quad (87)$$

$$A_t^{\text{anneal}}(j, i) := \beta A_t(j, i) \frac{p_t^{1-\beta}(j)}{p_t^{1-\beta}(i)}, \quad g_t(i) := \sum_{j \neq i} (A_t^{\text{anneal}}(i, j) - \beta A_t(i, j)). \quad (88)$$

From the definition of $q_t(i)$ we have

$$\sum_i q_t(i) = 1, \quad \forall t, \quad (89)$$

hence,

$$\sum_i \frac{\partial q_t(i)}{\partial t} = 0 \implies \sum_i q_t(i) \left(g_t(i) - \frac{\partial}{\partial t} \log Z_t \right) = 0, \quad (90)$$

which immediately yields

$$g_t(i) - \frac{\partial}{\partial t} \log Z_t = g_t(i) - \mathbb{E}_{i \sim q_t(i)} g_t(i). \quad (91)$$

However, one can also verify this through the definition of the normalization constant

$$\frac{\partial}{\partial t} \log Z_t = \frac{1}{Z_t} \sum_i \frac{\partial p_t^\beta(i)}{\partial t} = \sum_i \frac{p_t^\beta(i)}{Z_t} \beta \frac{\partial}{\partial t} \log p_t(i) \quad (92)$$

$$= \sum_i q_t(i) \sum_{j \neq i} \left(\beta A_t(j, i) \frac{p_t(j)}{p_t(i)} - \beta A_t(i, j) \right), \quad (93)$$

and, correspondingly

$$\sum_i q_t(i) g_t(i) - \frac{\partial}{\partial t} \log Z_t = \sum_i q_t(i) \sum_{j \neq i} \left(\beta A_t(i, j) \frac{p_t^{1-\beta}(i)}{p_t^{1-\beta}(j)} - \beta A_t(j, i) \frac{p_t(j)}{p_t(i)} \right) \quad (94)$$

$$= \frac{\beta}{Z_t} \sum_i \sum_{j \neq i} \left(A_t(i, j) \frac{p_t(i)}{p_t^{1-\beta}(j)} - A_t(j, i) \frac{p_t(j)}{p_t^{1-\beta}(i)} \right) \quad (95)$$

$$= \frac{\beta}{Z_t} \left(\sum_i \sum_{j \neq i} \hat{A}_t(i, j) - \sum_i \sum_{j \neq i} \hat{A}_t(j, i) \right) \quad (96)$$

$$= \frac{\beta}{Z_t} \left(\sum_{i,j} \hat{A}_t(i, j) - \sum_{i,j} \hat{A}_t(j, i) \right) = 0, \quad (97)$$

where we denote $\hat{A}_t(i, j) := A_t(i, j) \frac{p_t(i)}{p_t^{1-\beta}(j)}$.

Thus, we have

$$\frac{\partial q_t(i)}{\partial t} = \sum_{j \neq i} \left(A_t^{\text{anneal}}(j, i) q_t(j) - A_t^{\text{anneal}}(i, j) q_t(i) \right) + q_t(i) (g_t(i) - \mathbb{E}_{q_t(j)} g_t(j)), \quad (98)$$

$$A_t^{\text{anneal}}(j, i) := \beta A_t(j, i) \frac{p_t^{1-\beta}(j)}{p_t^{1-\beta}(i)}, \quad g_t(i) := \sum_{j \neq i} (A_t^{\text{anneal}}(i, j) - \beta A_t(i, j)). \quad (99)$$

□

Corollary C.1. [Annealed Masked Diffusion] *For the rate matrix of the reverse-time masked diffusion from Equation (10), Theorem 3.1 yields the following off-diagonal elements of the rate matrix and the corresponding weight function*

$$B_\tau^{\text{anneal}}(i, j) = -\delta_{mi} \frac{\beta}{\alpha_t} \frac{\partial \alpha_t}{\partial t} \frac{p_t^\beta(j)}{p_t^\beta(m)}, \quad g_\tau(i) = \delta_{mi} \frac{\beta}{\alpha_t} \frac{\partial \alpha_t}{\partial t} \sum_j \left(\frac{p_t(j)}{p_t(m)} - \frac{p_t^\beta(j)}{p_t^\beta(m)} \right). \quad (14)$$

Proof. The reverse-time rate matrix is

$$B_t(i, j) = -\delta_{mi} \frac{1}{\alpha_t} \frac{\partial \alpha_t}{\partial t} \frac{p_t(j)}{p_t(m)}, \quad i \neq j. \quad (100)$$

Then, according to Theorem 3.1, the rate matrix of the annealed process is

$$B_t^{\text{anneal}}(i, j) = \beta B_t(i, j) \frac{p_t^{1-\beta}(i)}{p_t^{1-\beta}(j)} = -\delta_{mi} \frac{\beta}{\alpha_t} \frac{\partial \alpha_t}{\partial t} \frac{p_t(j)}{p_t(m)} \frac{p_t^{1-\beta}(i)}{p_t^{1-\beta}(j)} = -\delta_{mi} \frac{\beta}{\alpha_t} \frac{\partial \alpha_t}{\partial t} \frac{p_t^\beta(j)}{p_t^\beta(m)} \quad (101)$$

And the weighting term is

$$g_t(i) = \sum_{j \neq i} (B_t^{\text{anneal}}(i, j) - \beta B_t(i, j)) = \delta_{mi} \frac{\beta}{\alpha_t} \frac{\partial \alpha_t}{\partial t} \sum_{j \neq i} \left(\frac{p_t(j)}{p_t(m)} - \frac{p_t^\beta(j)}{p_t^\beta(m)} \right) \quad (102)$$

$$= \delta_{mi} \frac{\beta}{\alpha_t} \frac{\partial \alpha_t}{\partial t} \sum_{j \neq m} \left(\frac{p_t(j)}{p_t(m)} - \frac{p_t^\beta(j)}{p_t^\beta(m)} \right) = \delta_{mi} \frac{\beta}{\alpha_t} \frac{\partial \alpha_t}{\partial t} \sum_j \left(\frac{p_t(j)}{p_t(m)} - \frac{p_t^\beta(j)}{p_t^\beta(m)} \right) \quad (103)$$

□

C.2 PRODUCT OF FKEs

Theorem 3.3. [Product of FKEs] *Consider two forward Kolmogorov equations (from Equation (2)) with different rate matrices $A_t^1(i, j)$ and $A_t^2(i, j)$ describing the evolution of marginals $p_t^1(i)$ and $p_t^2(i)$. For the product of marginals $q_t(i) \propto p_t^1(i)p_t^2(i)$, the following equation holds*

$$\frac{\partial q_t(i)}{\partial t} = \sum_{j \neq i} \left(A_t^{\text{prod}}(j, i)q_t(j) - A_t^{\text{prod}}(i, j)q_t(i) \right) + q_t(i)(g_t(i) - \mathbb{E}_{j \sim q_t(j)}g_t(j)), \quad (16)$$

$$A_t^{\text{prod}}(i, j) := A_t^1(i, j) \frac{p_t^2(j)}{p_t^2(i)} + A_t^2(i, j) \frac{p_t^1(j)}{p_t^1(i)}, \quad g_t(i) := \sum_{j \neq i} \left(A_t^{\text{prod}}(i, j) - A_t^1(i, j) - A_t^2(i, j) \right).$$

Proof. Consider two forward Kolmogorov equations with different rate matrices $A_t^1(i, j)$ and $A_t^2(i, j)$. For both we have the equations of the form

$$\frac{\partial p_t^{1,2}(i)}{\partial t} = \sum_{j \neq i} A_t^{1,2}(j, i)p_t^{1,2}(j) - \sum_{j \neq i} A_t^{1,2}(i, j)p_t^{1,2}(i) \quad (104)$$

$$\frac{\partial}{\partial t} \log p_t^{1,2}(i) = \sum_{j \neq i} A_t^{1,2}(j, i) \frac{p_t^{1,2}(j)}{p_t^{1,2}(i)} - \sum_{j \neq i} A_t^{1,2}(i, j) \quad (105)$$

$$= \sum_{j \neq i} \left(A_t^{1,2}(j, i) \frac{p_t^{1,2}(j)}{p_t^{1,2}(i)} - A_t^{1,2}(i, j) \right). \quad (106)$$

Correspondingly, for the density $q_t(i) := p_t^1(i)p_t^2(i)/Z_t$, we have

$$\frac{\partial}{\partial t} \log q_t(i) = \frac{\partial}{\partial t} \log p_t^1(i) + \frac{\partial}{\partial t} \log p_t^2(i) - \frac{\partial}{\partial t} \log Z_t \quad (107)$$

$$= \sum_{j \neq i} \left(A_t^1(j, i) \frac{p_t^1(j)}{p_t^1(i)} - A_t^1(i, j) + A_t^2(j, i) \frac{p_t^2(j)}{p_t^2(i)} - A_t^2(i, j) \right) - \frac{\partial}{\partial t} \log Z_t \quad (108)$$

$$= \sum_{j \neq i} \left(A_t^1(j, i) \frac{p_t^2(i)}{p_t^2(j)} \frac{q_t(j)}{q_t(i)} + A_t^2(j, i) \frac{p_t^1(i)}{p_t^1(j)} \frac{q_t(j)}{q_t(i)} - A_t^1(i, j) - A_t^2(i, j) \right) - \frac{\partial}{\partial t} \log Z_t \quad (109)$$

$$= \sum_{j \neq i} \left(\underbrace{\left[A_t^1(j, i) \frac{p_t^2(i)}{p_t^2(j)} + A_t^2(j, i) \frac{p_t^1(i)}{p_t^1(j)} \right]}_{:= A_t^{\text{prod}}(j, i)} \frac{q_t(j)}{q_t(i)} - A_t^1(i, j) - A_t^2(i, j) \right) - \frac{\partial}{\partial t} \log Z_t \quad (110)$$

$$= \sum_{j \neq i} \left(A_t^{\text{prod}}(j, i) \frac{q_t(j)}{q_t(i)} - A_t^{\text{prod}}(i, j) \right) + \quad (111)$$

$$+ \underbrace{\sum_{j \neq i} \left(A_t^{\text{prod}}(i, j) - A_t^1(i, j) - A_t^2(i, j) \right)}_{:= g_t(i)} - \frac{\partial}{\partial t} \log Z_t. \quad (112)$$

Finally, we have to show that the weights are self-normalized, i.e.

$$g_t(i) - \frac{\partial}{\partial t} \log Z_t = g_t(i) - \mathbb{E}_{i \sim q_t(j)} g_t(j). \quad (113)$$

Expanding the derivative of the normalization constant, we have

$$\begin{aligned} \frac{\partial}{\partial t} \log Z_t &= \frac{1}{Z_t} \sum_i \left(p_t^1(i) \frac{\partial p_t^2(i)}{\partial t} + p_t^2(i) \frac{\partial p_t^1(i)}{\partial t} \right) = \sum_i q_t(i) \left(\frac{\partial}{\partial t} \log p_t^2(i) + \frac{\partial}{\partial t} \log p_t^1(i) \right) \\ &= \sum_i q_t(i) \sum_{j \neq i} \left(A_t^1(j, i) \frac{p_t^1(j)}{p_t^1(i)} - A_t^1(i, j) + A_t^2(j, i) \frac{p_t^2(j)}{p_t^2(i)} - A_t^2(i, j) \right). \end{aligned} \quad (114)$$

Thus, we have

$$\begin{aligned} \sum_i q_t(i) g_t(i) - \frac{\partial}{\partial t} \log Z_t &= \sum_i q_t(i) \sum_{j \neq i} \left(A_t^{\text{prod}}(i, j) - A_t^1(j, i) \frac{p_t^1(j)}{p_t^1(i)} - A_t^2(j, i) \frac{p_t^2(j)}{p_t^2(i)} \right) \\ &= \sum_i q_t(i) \sum_{j \neq i} \left(A_t^1(i, j) \frac{p_t^2(j)}{p_t^2(i)} + A_t^2(i, j) \frac{p_t^1(j)}{p_t^1(i)} - A_t^1(j, i) \frac{p_t^1(j)}{p_t^1(i)} - A_t^2(j, i) \frac{p_t^2(j)}{p_t^2(i)} \right) \end{aligned} \quad (115)$$

$$= \frac{1}{Z_t} \sum_i \sum_{j \neq i} \left(A_t^1(i, j) p_t^1(i) p_t^2(j) + A_t^2(i, j) p_t^1(j) p_t^2(i) - \right. \quad (116)$$

$$\left. - A_t^1(j, i) p_t^1(j) p_t^2(i) - A_t^2(j, i) p_t^1(i) p_t^2(j) \right). \quad (117)$$

Denoting

$$\hat{A}_t(i, j) := A_t^1(i, j) p_t^1(i) p_t^2(j) + A_t^2(i, j) p_t^1(j) p_t^2(i), \quad (118)$$

we can show

$$\sum_i q_t(i) g_t(i) - \frac{\partial}{\partial t} \log Z_t = \frac{1}{Z_t} \sum_i \sum_{j \neq i} \left(\hat{A}_t(i, j) - \hat{A}_t(j, i) \right) \quad (119)$$

$$= \frac{1}{Z_t} \sum_{i, j} \left(\hat{A}_t(i, j) - \hat{A}_t(j, i) \right) = 0. \quad (120)$$

Thus, we have the result of the theorem, i.e.

$$\frac{\partial q_t(i)}{\partial t} = \sum_{j \neq i} \left(A_t^{\text{prod}}(j, i) q_t(j) - A_t^{\text{prod}}(i, j) q_t(i) \right) + q_t(i) (g_t(i) - \mathbb{E}_{j \sim q_t(j)} g_t(j)), \quad (121)$$

$$\text{where } A_t^{\text{prod}}(i, j) := A_t^1(i, j) \frac{p_t^2(j)}{p_t^2(i)} + A_t^2(i, j) \frac{p_t^1(j)}{p_t^1(i)}, \quad (122)$$

$$g_t(i) := \sum_{j \neq i} \left(A_t^{\text{prod}}(i, j) - A_t^1(i, j) - A_t^2(i, j) \right). \quad (123)$$

□

Corollary C.2. [Product of Masked Diffusions] *For the rate matrix of the reverse-time masked diffusion from Equation (10), Theorem 3.3 yields*

$$B_\tau^{\text{prod}}(i, j) = -2\delta_{mi} \frac{1}{\alpha_t} \frac{\partial \alpha_t}{\partial t} \frac{p_t^1(j)}{p_t^1(m)} \frac{p_t^2(j)}{p_t^2(m)}, \quad g_\tau(i) = \frac{\delta_{mi}}{\alpha_t} \frac{\partial \alpha_t}{\partial t} \sum_j \frac{p_t^1(j)}{p_t^1(m)} + \frac{p_t^2(j)}{p_t^2(m)} - 2 \frac{p_t^1(j)}{p_t^1(m)} \frac{p_t^2(j)}{p_t^2(m)}$$

Proof. The reverse-time rate matrices are

$$B_t^1(i, j) = -\delta_{mi} \frac{1}{\alpha_t} \frac{\partial \alpha_t}{\partial t} \frac{p_t^1(j)}{p_t^1(m)}, \quad B_t^2(i, j) = -\delta_{mi} \frac{1}{\alpha_t} \frac{\partial \alpha_t}{\partial t} \frac{p_t^2(j)}{p_t^2(m)}. \quad (124)$$

Then, according to Theorem 3.3, the rate matrix for the product is

$$B_t^{\text{prod}}(i, j) = B_t^1(i, j) \frac{p_t^2(j)}{p_t^2(i)} + B_t^2(i, j) \frac{p_t^1(j)}{p_t^1(i)} \quad (125)$$

$$= -\delta_{mi} \frac{1}{\alpha_t} \frac{\partial \alpha_t}{\partial t} \frac{p_t^1(j)}{p_t^1(m)} \frac{p_t^2(j)}{p_t^2(i)} - \delta_{mi} \frac{1}{\alpha_t} \frac{\partial \alpha_t}{\partial t} \frac{p_t^2(j)}{p_t^2(m)} \frac{p_t^1(j)}{p_t^1(i)} \quad (126)$$

$$= -\delta_{mi} \frac{2}{\alpha_t} \frac{\partial \alpha_t}{\partial t} \frac{p_t^1(j)}{p_t^1(m)} \frac{p_t^2(j)}{p_t^2(m)}. \quad (127)$$

And the weighting term is

$$g_t(i) = \sum_{j \neq i} \left(B_t^{\text{prod}}(i, j) - B_t^1(i, j) - B_t^2(i, j) \right) \quad (128)$$

$$= \delta_{mi} \frac{1}{\alpha_t} \frac{\partial \alpha_t}{\partial t} \sum_j \left(\frac{p_t^1(j)}{p_t^1(m)} + \frac{p_t^2(j)}{p_t^2(m)} - 2 \frac{p_t^1(j)}{p_t^1(m)} \frac{p_t^2(j)}{p_t^2(m)} \right). \quad (129)$$

□

C.3 GEOMETRIC AVERAGE OF FKEs

Theorem C.3. [Geometric Average of FKEs] *Consider N forward Kolmogorov equations with marginals $p_t^n(i)$ and corresponding rate matrices $A_t^n(i, j)$. For the geometric average of marginals $q_t(i) \propto \prod_{n=1}^N p_t^n(i)^{\beta_n}$, with $\sum_{i=1}^N \beta_n = 1$, the following equation holds*

$$\frac{\partial q_t(i)}{\partial t} = \sum_{j \neq i} \left(A_t^{\text{geom}}(j, i) q_t(j) - A_t^{\text{geom}}(i, j) q_t(i) \right) + q_t(i) (g_t(i) - \mathbb{E}_{q_t(j)} g_t(j)), \quad (130)$$

$$\text{where } A_t^{\text{geo}}(i, j) := \prod_{n=1}^N \left(\frac{p_t^n(j)}{p_t^n(i)} \right)^{\beta_n} \sum_{n=1}^N \beta_n A_t^n(j, i) \frac{p_t^n(j)}{p_t^n(i)}, \quad (131)$$

$$g_t(i) := \sum_{j \neq i} \left(A_t^{\text{geo}}(i, j) - \sum_{n=1}^N \beta_n A_t^n(i, j) \right). \quad (132)$$

Proof. We define the target marginals as

$$q_t(i) := \frac{1}{Z_t} \prod_{n=1}^N p_t^n(i)^{\beta_n}, \quad Z_t = \sum_i \prod_{n=1}^N p_t^n(i)^{\beta_n}. \quad (133)$$

Hence, the time derivative of the marginals is

$$\frac{\partial}{\partial t} \log q_t(i) = \sum_{n=1}^N \beta_n \frac{\partial}{\partial t} \log p_t^n(i) - \frac{\partial}{\partial t} \log Z_t \quad (134)$$

$$= \sum_{j \neq i} \sum_{n=1}^N \beta_n \left(A_t^n(j, i) \frac{p_t^n(j)}{p_t^n(i)} - A_t^n(i, j) \right) - \frac{\partial}{\partial t} \log Z_t \quad (135)$$

$$= \sum_{j \neq i} \left(\underbrace{\sum_{n=1}^N \beta_n A_t^n(j, i) \frac{p_t^n(j)}{p_t^n(i)} \frac{q_t(i)}{q_t(j)} \frac{q_t(j)}{q_t(i)}}_{:= A_t^{\text{geom}}(j, i)} - A_t^{\text{geom}}(i, j) \right) + \quad (136)$$

$$+ \sum_{j \neq i} \left(A_t^{\text{geom}}(i, j) - \sum_{n=1}^N \beta_n A_t^n(i, j) \right) - \frac{\partial}{\partial t} \log Z_t. \quad (137)$$

Denoting

$$A_t^{\text{geom}}(i, j) := \prod_{n=1}^N \left(\frac{p_t^n(j)}{p_t^n(i)} \right)^{\beta_n} \sum_{n=1}^N \beta_n A_t^n(i, j) \frac{p_t^n(i)}{p_t^n(j)}, \text{ and} \quad (138)$$

$$g_t(i) := \sum_{j \neq i} \left(A_t^{\text{geom}}(i, j) - \sum_{n=1}^N \beta_n A_t^n(i, j) \right), \quad (139)$$

we can describe the evolution of the marginals $q_t(i)$ as

$$\frac{\partial q_t(i)}{\partial t} = \sum_{j \neq i} (A_t^{\text{geom}}(j, i) q_t(j) - A_t^{\text{geom}}(i, j) q_t(i)) + q_t(i) (g_t(i) - \mathbb{E}_{j \sim q_t(j)} g_t(j)). \quad (140)$$

□

Corollary C.4. [Geometric Average of Masked Diffusions] *For the rate matrix of the reverse-time masked diffusion from Equation (10), Theorem C.3 yields*

$$B_t^{\text{geom}}(i, j) = -\delta_{mi} \frac{1}{\alpha_t} \frac{\partial \alpha_t}{\partial t} \prod_{n=1}^N \left(\frac{p_t^n(j)}{p_t^n(m)} \right)^{\beta_n}, \quad i \neq j \quad (141)$$

$$g_t(i) = \delta_{mi} \frac{1}{\alpha_t} \frac{\partial \alpha_t}{\partial t} \sum_{j \neq i} \left(\sum_{n=1}^N \beta_n \frac{p_t^n(j)}{p_t^n(m)} - \prod_{n=1}^N \left(\frac{p_t^n(j)}{p_t^n(m)} \right)^{\beta_n} \right). \quad (142)$$

Proof. For the reverse-time masked diffusion, we have

$$B_t^n(i, j) = -\delta_{mi} \frac{1}{\alpha_t} \frac{\partial \alpha_t}{\partial t} \frac{p_t^n(j)}{p_t^n(m)}, \quad i \neq j, \quad n = 1, \dots, N. \quad (143)$$

Using the result of Theorem C.3, we have

$$B_t^{\text{geom}}(i, j) = -\delta_{mi} \frac{1}{\alpha_t} \frac{\partial \alpha_t}{\partial t} \prod_{n=1}^N \left(\frac{p_t^n(j)}{p_t^n(i)} \right)^{\beta_n} \sum_{n=1}^N \beta_n B_t^n(i, j) \frac{p_t^n(i)}{p_t^n(j)} \quad (144)$$

$$= -\delta_{mi} \frac{1}{\alpha_t} \frac{\partial \alpha_t}{\partial t} \prod_{n=1}^N \left(\frac{p_t^n(j)}{p_t^n(i)} \right)^{\beta_n} \sum_{n=1}^N \beta_n \frac{p_t^n(j)}{p_t^n(m)} \frac{p_t^n(i)}{p_t^n(j)} \quad (145)$$

$$= -\delta_{mi} \frac{1}{\alpha_t} \frac{\partial \alpha_t}{\partial t} \prod_{n=1}^N \left(\frac{p_t^n(j)}{p_t^n(m)} \right)^{\beta_n}, \quad (146)$$

where in the last transition we have used the fact that the expression is zero unless $i = m$ and $\sum_{n=1}^N \beta_n = 1$. Correspondingly, the weights are

$$g_t(i) = \sum_{j \neq i} \left(B_t^{\text{geom}}(i, j) - \sum_{n=1}^N \beta_n B_t^n(i, j) \right) \quad (147)$$

$$= \delta_{mi} \frac{1}{\alpha_t} \frac{\partial \alpha_t}{\partial t} \sum_{j \neq i} \left(\sum_{n=1}^N \beta_n \frac{p_t^n(j)}{p_t^n(m)} - \prod_{n=1}^N \left(\frac{p_t^n(j)}{p_t^n(m)} \right)^{\beta_n} \right). \quad (148)$$

□

C.4 REWARD-TILTED FKE

Theorem 3.5. [Reward-tilted FKE] Consider the forward Kolmogorov equation from Equation (2) describing the time evolution of the marginals $p_t(i)$ with the rate matrix $A_t(i, j)$. For the reward-tilted marginals $q_t(i) \propto p_t(i) \exp(\beta_t r(i))$, the following equation holds

$$\frac{\partial q_t(i)}{\partial t} = \sum_{j \neq i} \left(A_t^{\text{reward}}(j, i) q_t(j) - A_t^{\text{reward}}(i, j) q_t(i) \right) + q_t(i) (g_t(i) - \mathbb{E}_{q_t(j)} g_t(j)), \quad (17)$$

$$A_t^{\text{reward}}(i, j) := A_t(i, j) \frac{\exp(\beta_t r(j))}{\exp(\beta_t r(i))}, \quad g_t(i) := \sum_{j \neq i} \left(A_t^{\text{reward}}(i, j) - A_t(i, j) \right) + \frac{\partial \beta_t}{\partial t} r(i). \quad (18)$$

Proof. We define

$$q_t(i) := \frac{1}{Z_t} p_t(i) \exp(\beta_t r(i)), \quad Z_t = \sum_i p_t(i) \exp(\beta_t r(i)) \quad (149)$$

The derivative of the log-probability is

$$\frac{\partial}{\partial t} \log q_t(i) = \sum_{j \neq i} \left(A_t(j, i) \frac{p_t(j)}{p_t(i)} - A_t(i, j) \right) + \frac{\partial \beta_t}{\partial t} r(i) - \frac{\partial}{\partial t} \log Z_t \quad (150)$$

$$= \sum_{j \neq i} \left(\underbrace{A_t(j, i) \frac{\exp(\beta_t r(i))}{\exp(\beta_t r(j))} \frac{q_t(j)}{q_t(i)}}_{:= A_t^{\text{reward}}(j, i)} - A_t(i, j) \right) + \frac{\partial \beta_t}{\partial t} r(i) - \frac{\partial}{\partial t} \log Z_t \quad (151)$$

$$= \sum_{j \neq i} \left(A_t^{\text{reward}}(j, i) \frac{q_t(j)}{q_t(i)} - A_t^{\text{reward}}(i, j) \right) + \quad (152)$$

$$+ \underbrace{\sum_{j \neq i} (A_t^{\text{reward}}(i, j) - A_t(i, j)) + \frac{\partial \beta_t}{\partial t} r(i) - \frac{\partial}{\partial t} \log Z_t}_{:= g_t(i)} \quad (153)$$

To show the following equality

$$g_t(i) - \frac{\partial}{\partial t} \log Z_t = g_t(i) - \mathbb{E}_{i \sim q_t(j)} g_t(j), \quad (154)$$

one can either use the definition of $q_t(i)$ and its normalization, or explicitly calculate the derivative of the normalizing constant, i.e.

$$\frac{\partial}{\partial t} \log Z_t = \frac{1}{Z_t} \sum_i \frac{\partial}{\partial t} (p_t(i) \exp(\beta_t r(i))) \quad (155)$$

$$= \sum_i q_t(i) \left(\frac{\partial}{\partial t} \log p_t(i) + \frac{\partial \beta_t}{\partial t} r(i) \right) \quad (156)$$

$$= \sum_i q_t(i) \left(\sum_{j \neq i} \left(A_t(j, i) \frac{p_t(j)}{p_t(i)} - A_t(i, j) \right) + \frac{\partial \beta_t}{\partial t} r(i) \right) \quad (157)$$

Thus, we have

$$\sum_i q_t(i) g_t(i) - \frac{\partial}{\partial t} \log Z_t = \sum_i q_t(i) \left(\left(\sum_{j \neq i} A_t^{\text{reward}}(i, j) - A_t(i, j) \right) + \frac{\partial \beta_t}{\partial t} r(i) \right) \quad (158)$$

$$- \left(\sum_{j \neq i} A_t(j, i) \frac{p_t(j)}{p_t(i)} - A_t(i, j) \right) - \frac{\partial \beta_t}{\partial t} r(i) \quad (159)$$

$$= \sum_i q_t(i) \sum_{j \neq i} \left(A_t^{\text{reward}}(i, j) - A_t(j, i) \frac{p_t(j)}{p_t(i)} \right) \quad (160)$$

$$= \sum_i q_t(i) \sum_{j \neq i} \left(A_t(i, j) \frac{\exp(\beta_t r(j))}{\exp(\beta_t r(i))} - A_t(j, i) \frac{p_t(j)}{p_t(i)} \right) \quad (161)$$

$$= \frac{1}{Z_t} \sum_i \sum_{j \neq i} \left(A_t(i, j) \exp(\beta_t r(j)) p_t(i) - A_t(j, i) \exp(\beta_t r(i)) p_t(j) \right) \quad (162)$$

$$= \frac{1}{Z_t} \sum_i \sum_{j \neq i} \left(\hat{A}_t(i, j) - \hat{A}_t(j, i) \right) = \frac{1}{Z_t} \sum_{i, j} \left(\hat{A}_t(i, j) - \hat{A}_t(j, i) \right) = 0, \quad (163)$$

where we denote

$$\hat{A}_t(i, j) := A_t(i, j) \exp(\beta_t r(j)) p_t(i). \quad (164)$$

Finally, we have

$$\frac{\partial q_t(i)}{\partial t} = \sum_{j \neq i} (A_t^{\text{reward}}(j, i) q_t(j) - A_t^{\text{reward}}(i, j) q_t(i)) + q_t(i) (g_t(i) - \mathbb{E}_{j \sim q_t(j)} g_t(j)), \quad (165)$$

$$A_t^{\text{reward}}(i, j) := A_t(i, j) \frac{\exp(\beta_t r(j))}{\exp(\beta_t r(i))}, \quad g_t(i) := \sum_{j \neq i} \left(A_t^{\text{reward}}(i, j) - A_t(i, j) \right) + \frac{\partial \beta_t}{\partial t} r(i).$$

□

Corollary C.5. [Reward-tilted Masked Diffusion] *For the rate matrix of the reverse-time masked diffusion from Equation (10), Theorem 3.5 yields*

$$B_\tau^{\text{reward}}(i, j) = -\delta_{mi} \frac{1}{\alpha_t} \frac{\partial \alpha_t}{\partial t} \frac{p_t(j)}{p_t(m)} \frac{\exp(\beta_t r(j))}{\exp(\beta_t r(m))}, \quad (19)$$

$$g_\tau(i) = \frac{1}{\alpha_t} \frac{\partial \alpha_t}{\partial t} \delta_{mi} \sum_j \left(\frac{p_t(j)}{p_t(m)} - \frac{p_t(j)}{p_t(m)} \frac{\exp(\beta_t r(j))}{\exp(\beta_t r(m))} \right) + \frac{\partial \beta_t}{\partial t} r(i). \quad (20)$$

Proof. The reverse-time rate matrix is

$$B_t(i, j) = -\delta_{mi} \frac{1}{\alpha_t} \frac{\partial \alpha_t}{\partial t} \frac{p_t(j)}{p_t(m)}. \quad (166)$$

Then the reward-weighted matrix is

$$B_t^{\text{reward}}(i, j) = B_t(i, j) \frac{\exp(\beta_t r(j))}{\exp(\beta_t r(i))} = -\delta_{mi} \frac{1}{\alpha_t} \frac{\partial \alpha_t}{\partial t} \frac{p_t(j)}{p_t(m)} \frac{\exp(\beta_t r(j))}{\exp(\beta_t r(m))}, \quad (167)$$

and the weighting term is

$$g_t(i) = \sum_{j \neq i} (B_t^{\text{reward}}(i, j) - B_t(i, j)) + \frac{\partial \beta_t}{\partial t} r(i) \quad (168)$$

$$= \delta_{mi} \frac{1}{\alpha_t} \frac{\partial \alpha_t}{\partial t} \sum_j \left(\frac{p_t(j)}{p_t(m)} - \frac{p_t(j)}{p_t(m)} \frac{\exp(\beta_t r(j))}{\exp(\beta_t r(m))} \right) + \frac{\partial \beta_t}{\partial t} r(i) \quad (169)$$

□

D EXPERIMENTAL DETAILS

Code is available at https://github.com/hasanmohsin/discrete_fkc

D.1 ANNEALING THE ISING MODEL

The settings for various experiments are outlined below.

Dataset for experiment 1

```
source: synthetic Ising model configurations
size: 200,000 samples after burn-in
sampling method: Swendsen-Wang
    burn-in length: 10,000 steps
    thinning interval: 5
beta: 0.3
lattice size: 16
```

Dataset for experiment 2

```
source: synthetic Ising model configurations
size: 10,000 samples after burn-in
sampling method: Glauber dynamics
    burn-in length: 10,000 steps
    thinning interval: 1
beta: 0.2 and 0.3
lattice size: 16
```

Model

```
architecture: UNet
activation: SiLU
channels: [16, 32, 64]
resblocks per stage: 2
attention: applied at 4×4 resolution
initialization: Xavier uniform
time embedding: sinusoidal embedding
```

Training

```
optimizer: AdamW
    learning rate: 2e-4
    betas: (0.9, 0.999)
    weight_decay: 1e-4
batch size: 400
epochs: 6000
learning rate schedule: constant with warmup
hardware: 1 × NVIDIA A100 GPU (40 GB memory)
loss: denoising score entropy
```

Evaluation

```
metrics for global structure: 2-Wasserstein metric between
distributions of
energy and distributions of magnetization.
metrics for local structure: MSE for correlation function.
sample size: 10,000
```

The hyperparameters searched over are outlined below.

```
optimizer:
    learning rate: [5e-5, 1e-4, 2e-4, 3e-4, 4e-4, 1e-3]
```

```

  weight_decay: [0, 5e-5, 1e-4, 2e-4, 5e-4, 1e-3]
batch size: [100, 200, 400, 800, 1600]
model:
  UNet base channels: [16,32,64,128,256]
  time embedding size: [16,32,64,128,256]
  rate matrix time dependence: [linear, sine]
method:
  Number of particles: [100, 1000, 5000, 10000]
  Number of steps: [500, 1000, 2000, 5000]

```

Hyperparameters were selected based on Wasserstein-2 distance between samples and Swendsen-Wang distance for energy distribution. For the DFKC method itself we looked at number of steps and number of particles as hyperparameters.

D.2 AMORTIZED LINEAR REGRESSION

D.2.1 THEORETICAL JUSTIFICATION

The posterior over parameters factors as:

$$p(\theta|\mathcal{X}) \propto p(\theta)p(\mathcal{X}|\theta) = p(\theta) \prod_k^K p(\mathcal{X}_k|\theta) \propto p(\theta)^{1-K} \prod_k^K p(\theta|\mathcal{X}_k) \quad (170)$$

For a uniform prior $p(\theta)$, this results in the product we applied $p(\theta|\mathcal{X}) \propto \prod_{k=1}^K p(\theta|\mathcal{X}_k)$.

D.2.2 EXPERIMENTAL SETUP

All experiments were done on a single A100 GPU.

For each experiment, the dataset \mathcal{X} was generated using $(\theta_0, \theta_1) = (3.0, 4.0)$, with x spaced linearly between $[-10, 10]$, and $y_i = \theta_1^* x_i + \theta_0^* + \epsilon$, where $\epsilon \sim \mathcal{N}(0, 0.1^2)$.

For inference with LLaDA, a temperature of 1.0 was used, and the random remasking strategy was applied. All predictions were made in a single block, and the generation length was capped at 128 tokens.

The number of SMC samples were selected based on MSE, for a fixed dataset size, over a grid of $\{2, 4, 5, 8, 16, 32\}$. 5 SMC samples were selected for evaluation.

The prompt used to generate predictions is of the form: "Assume a model of the form $y = a * x + b$, where a and b are the parameters of the model. The observations are given as (x, y) points, where y has Gaussian noise with standard deviation 0.1 added. Predict the parameters of linear regression for (x, y) points: " + (x_1, y_1) , ..., (x_N, y_N) + " Output the final answer as: "The best estimate for parameters of the model are: $a = \underline{}$, and $b = \underline{}$ " where $\underline{}$ is replaced with the values of a and then b ."

The generated data varied for different seeds, meaning that different seeds resulted in different prompts.

D.2.3 ADDITIONAL RESULTS FOR AMORTIZED LEARNING

We include an ablation over the number of SMC samples, for a fixed number of products in Figure A1. We can observe that more SMC samples improves performance, up to a threshold of 8 samples.

We additionally include a comparison of how well the outputs adhered to the specified prompt format in Figure A2.

Some selected samples from the product and joint prompting strategies are included in Table A3. We can note that outputs using joint prompting often fail to adhere to the output format specified in the prompt, and sometimes cannot be parsed for values of (θ_0, θ_1) . This issue wasn't observed for the product prompt (using any number of particles).

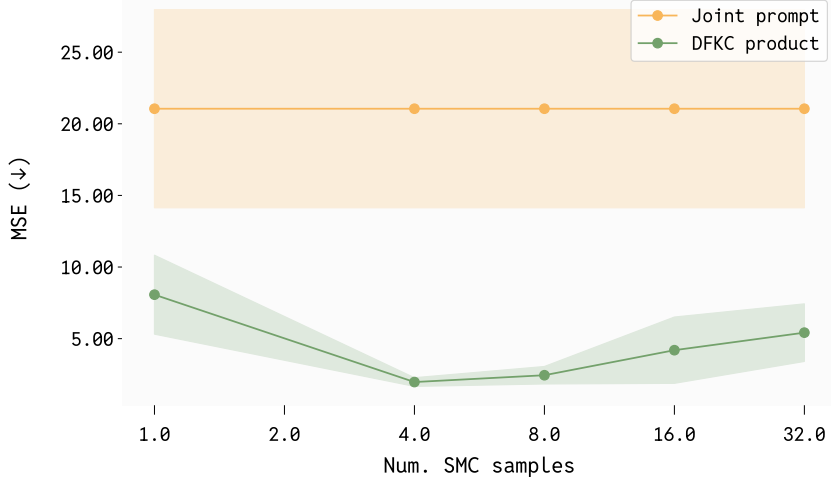


Figure A1: Increasing the number of SMC samples for DFKC improves over no SMC resampling; gain is largest with 4 or 8 samples. Taking the product has a lower (better) mean squared error (MSE) than joint prompting, and resampling with DFKC significantly improves this further.

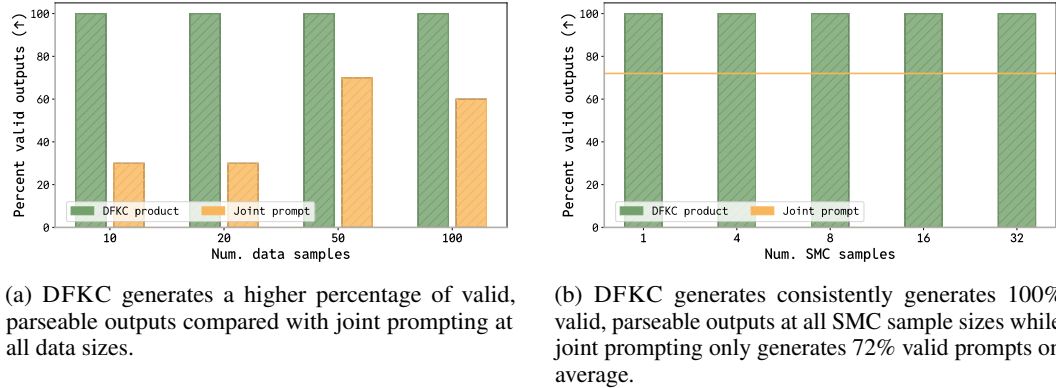


Figure A2: Effect of data quantity on predicting linear regression parameters.

D.3 CODE GENERATION

All experiments were done on an A100L GPU.

For evaluation, the HumanEval (Chen et al., 2021) and MBPP (Austin et al., 2021) coding datasets were used. For MBPP the sanitized dataset split was evaluated. For MBPP, the prompt was modified to add the function definition.

Evaluation consisted of computing average accuracy on test-cases provided in the dataset. For evaluation, the longest code segment in the generated output without any syntactic errors was parsed and sanitized.

Hyperparameters consisted of the number of SMC samples M , and inverse-temperature β . These were selected through search in a grid of $M = \{2, 4, 8\}$ and $\beta = \{3.0, 5.0, 10.0, 20.0\}$. Additionally, a remasking strategy of ‘low confidence’ or ‘random’ was evaluated on the hold-out set. The selection was performed based on accuracy on a small validation set (10 prompts from each dataset). For HumanEval, the final results were computed with $M = 4$, $\beta = 10.0$, and random remasking. For MBPP, the final results were computed with $M = 4$, $\beta = 20.0$, and random remasking.

The final evaluation results are reported on the remainder of the dataset (154 datapoints for HumanEval, and 417 points for MBPP).

A generation length of 128 was used for all experiments.

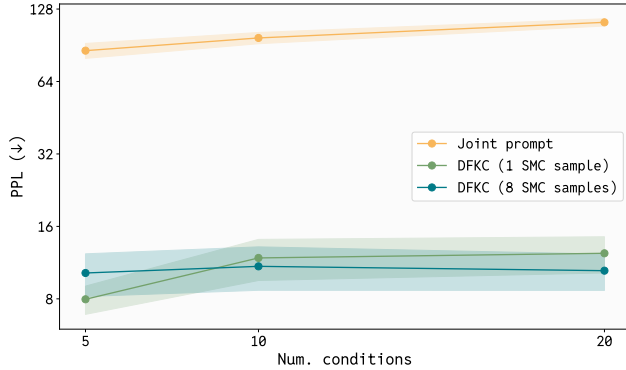


Figure A3: Multi-constraint story generation task: Comparison of Perplexity (PPL), between joint prompting, DFKC (1 SMC sample), and DFKC (8 SMC samples), for different numbers of conditions.

A table of results is included in Table A4 (the same values which were plotted in Figure 4). We note that “Naive Annealing” is equivalent to our method with 1 SMC sample (eg. without resampling). The improvement between our method and Naive Annealing therefore demonstrates the importance of resampling.

Table A4: Accuracy on coding tasks, with standard error reported over 5 seeds

Method	Human Eval (%)	MBPP (%)
Base Model	12.83 ± 0.38	10.00 ± 0.25
Base Model Argmax	30.74 ± 0.76	30.28 ± 0.87
Naive Annealing	30.49 ± 0.49	29.24 ± 1.07
DFKC (Ours)	33.78 ± 0.97	31.00 ± 0.40

D.4 MULTI-CONSTRAINT STORY GENERATION

We evaluate the product formulation for generating stories. For this task we prompt the language model to generate a story, with a list of constraints $C = \cup_k C_k$. Constraints may demand the inclusion of particular events or characters (such as a “hungry cat”), or be stylistic in nature (“the story should have mystery”). We use our method to sample from the product over individual constraints, and evaluate our adherence to the constraints by using the perplexity of the output under a more powerful language model, Qwen2.5 (Yang et al., 2024). Results for our method, over a varying number of constraints K , are included in Figure A3.

All experiments were performed on a single L40 GPU.

For inference with LLaDA, the next token to unmask was chosen randomly (as opposed to picking highest confidence one) due to the model frequently sampling end of text tokens using the latter setting. All experiments used a temperature of $T = 1.0$, and was generated within a single block with generation length L varying based on the number of constraints C (to account for the increasing complexity of the task as C grows). In particular:

$$L = \begin{cases} 128, & C \leq 6 \\ 256, & 6 < C \end{cases} \quad (171)$$

The prompt for the story generation is composed as follows: the base prompt is “Write a story.”. The conditions are sampled at random from a set of 50 conditions, containing mutually compatible constraints such as:

1. “It should include a curious child.”
2. “It should describe a small village.”
3. “It should feature a dense forest.”

4. . .

The number of SMC samples was selected by optimizing for PPL over a grid of $\{4, 8, 12\}$. The final results were computed with 8 samples.

Different seeds resulted in a different set of constraints being sampled to form the prompt.

D.5 PROTEIN SEQUENCE GENERATION

All experiments were done on a single L40 GPU.

The base discrete diffusion model used is DPLM1 650M (Wang et al., 2024b). For a sequence of length l , l generation steps are used, and once a token is unmasked, it is not remasked in future steps (to align more closely to the traditional masked diffusion generation process, and as opposed to the remasking strategies used in (Wang et al., 2024b)).

For each method we generate 50 samples per sequence length (in $\{10, 50, 100\}$), using all samples produced by any SMC algorithms. For instance, for FK Steering or DFKC with 5 particles, the set of 50 samples consist of 10 independent groups of 5 samples generated through the appropriate SMC algorithm. The results in Table 2 and Table A6 are computed through averages over these samples for all sequence lengths. We note that within an SMC run there may be multiple copies of a sequence, duplicated by the resampling mechanism (for FK Steering and DFKC).

To give a more comprehensive picture of the generated sequences for each method, in Table A5 we have reported reward values obtained by i) choosing the maximum reward sample from each SMC run (or for the non-SMC methods: the maximum reward sample among a group of 10 sequences), and ii) the mean reward over unique samples (ie. discarding any duplicates).

For the ESM2 likelihood reward, the SMC methods (FK Steering and DFKC) don't resample in the final 5% of sampling steps, which we found helped prevent collapse to a single sample. Such a modification was not needed for the Thermostability reward.

D.5.1 REWARD MODELS

ESM2 Likelihood Reward. The reward for a sequence x with length L is defined as the pseudo log-likelihood of the ESM2 model. This model takes a sequence as input, and outputs log-probabilities over the vocabulary for each token position, $\log p_\theta(y | x) \in \mathbb{R}^{V \times L}$. Classically, the pseudo log-likelihood (PLL) of such a model is calculated as:

$$\text{PLL}(x) = \frac{1}{L} \sum_{i=1}^L \log p_\theta(y_i = x_i | x_{\setminus i}) \quad (172)$$

Where $\log p_\theta(\cdot | x_{\setminus i})$ does a forward pass of the model while masking the token at position i . This is expensive since it requires a number of forward passes equivalent to the length of the sequence L . Gordon et al. (2025) propose a method of estimating the PLL using a single forward pass. First probabilities are computed on the complete sequence (without masking any positions): $p_i = p_\theta(y_i = x_i | x)$. Then these are transformed to calculate:

$$\hat{\text{PLL}}(x) = \frac{1}{L} \sum_{i=1}^L \log \left(\max \left(\frac{\alpha + \beta}{\alpha} p_i - \frac{\beta}{\alpha}, \epsilon \right) \right) \quad (173)$$

Where α, β are parameters related to the training of the model ($\alpha = \beta = 0.1$ for ESM2), and $\epsilon > 0$ is a small constant to prevent negative values.

For our unconditional experiments, the reward is computed with the latter formula, $r(x) = \hat{\text{PLL}}(x)$.

Thermostability Reward. We use a fine-tuned version of DPLM-650M which predicts thermostability from sequences. This model was evaluated to have a 0.695 Spearman correlation (see Table 1 of Wang et al. (2024a)). The reward $r(x)$ is the log of the predicted thermostability value.

The reward is scaled by a hyperparameter $\gamma > 0$ to compute the values used in the algorithm (for guidance and weight calculations): $\tilde{r}(x) = \gamma r(x)$ (so that we sample approximately from marginals $q_t(i) \propto p_t(i) \exp(\beta_t \tilde{r}(i))$).

In our results for unconditional protein generation, we set the reward-scale as $\gamma = 10$ for both the ESM2 and thermostability rewards, but report the unscaled reward $r(x)$ in tables and figures.

For partially masked sequences x , the reward is computed by first denoising x to a completely unmasked sequence x_0 by sampling from the denoiser (in a single step), and then evaluating the reward on x_0 . That is: $r(x) := r(x_0)$, $x_0 \sim p_\theta(x_0|x_t = x)$ (where $p_\theta(x_0|x_t)$ is the denoiser distribution, not the exact posterior).

Evaluating the reward ratio in Theorem 3.5 requires computing the reward on all neighbors of x (sequences that differ from x at a single token position). In this case, two choices are made to make the calculation more tractable:

1. The token position to unmask is chosen prior to computing the reward terms, from the base processes rate matrix (and logits). This means that the reward ratio only needs to be computed on neighbors differing from x on the chosen token position (for a vocabulary of size V , and length L , this reduces the number of reward evaluations from LV to V).
2. In computing the reward $r(x')$ on a partially masked neighbor x' : we do not unmask it using a separate call to the denoiser, instead all masked positions in x' are replaced with the corresponding tokens from $x_0 \sim p_\theta(x_0|x_t = x)$, ie. with the denoiser called on the sequence x . This is an approximation to computing $x'_0 \sim p(x'_0|x_t = x')$, and avoids multiple calls to the denoiser.

A linear annealing schedule $\beta_t = 1 - t$ is used for the reward (where generation starts at $t = 1$ and proceeds to $t = 0$).

D.5.2 BASELINES

DG-Exact. [(Nisonoff et al., 2024)] This method is equivalent to DFKC without resampling (or equivalently, with 1 SMC sample). Hyperparameters are set the same as our method.

FK Steering. [(Singhal et al., 2025)] The FK steering baseline uses the base model as the proposal, and uses the difference potential for resampling. The main hyperparameter involved is the number of SMC samples (M). The method is evaluated for $M = 5$ and $M = 10$, and the best performance for each reward is selected and reported in Table 2.

D.5.3 DESCRIPTION OF PROTEIN METRICS

Diversity. The "sequence diversity" metric of the generated sequences was obtained by normalizing the global pairwise sequence alignment. The metric serves to quantify how different the sampled sequences are.

Another metric for sequence diversity, "Max cluster", was evaluated using MMseqs2 clustering (Steinegger & Söding, 2017). Generated sequences were clustered with mmseqs easy-cluster using a 50% sequence identity threshold, 80% coverage, and cov-mode 0 (mmseqs easy-cluster --min-seq-id 0.5 -c 0.8 --cov-mode 0). Each cluster represents a group of related variants; we measured diversity as the fraction of clusters formed divided by the total number of sequences.

Structural confidence. To assess structural plausibility and quality, we used ESMFold (Lin et al., 2022) to predict a structure for each sequences and then computed both the average predicted local distance difference test (pLDDT) and predicted TM (pTM) score. pLDDT estimates how confident the model is in the local geometry at each residue, and pTM predicts how correct the overall topology is. High-confidence structures are considered to be those with pLDDT > 0.7; we also report this fraction.

Novelty. For each sequence, the structure was computed, and FoldSeek (van Kempen et al., 2024) was used to compute the TM-scores (Zhang & Skolnick, 2004) against a database of known structures from PDB ⁴ using the settings:

```
foldseek easy-search ... --format-output query,target,alntmscore
--alignment-type 1 --tmscore-threshold 0.0
```

⁴<https://github.com/steineggerlab/foldseek>

The reported novelty metrics include the maximum TM-score (lower is better, since it implies less alignment with database structures), and the fraction of structures with a maximum TM-score below 0.5, which suggests that they do not have general folds similar to those in the database (Xu & Zhang, 2010).

D.5.4 HYPERPARAMETERS

The main hyperparameters consisted of the reward scale γ , and the number of SMC samples used in DFKC and FK Steering. The reward scale was selected by evaluating the average (unscaled) reward on a set of generated sequences of smaller length (10, and 20), for $\gamma \in \{1.0, 5.0, 10.0, 50.0, 100.0, 200.0\}$. For the number of SMC samples, we evaluated the relevant methods with 5 and 10 samples, with results written in Table A6. The results for the best performing number of samples for each method was selected and reported in Table 2.

D.5.5 ADDITIONAL PROTEIN RESULTS

In Figure A4 we plot the protein rewards (both ESM2 likelihood and thermostability) along the evaluated sequence lengths and along different numbers of SMC samples for DFKC. We observe that going to 5 particles from 1 particle (without resampling, which is equivalent to the guidance method referred to as DG-Exact in (Nisonoff et al., 2024)) improves the reward. We note that our method generally outperforms the base model and DG-Exact.

We report the protein metrics for the ESM2 likelihood and Thermostability tasks, varying the number of SMC samples for FK Steering and DFKC, in Table A6. The highest reward settings for each method was reported in Table 2.

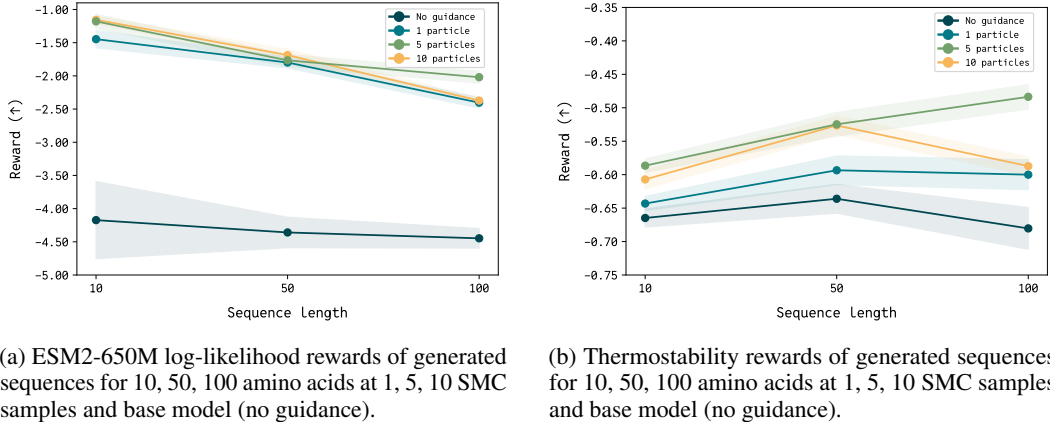


Figure A4: DFKC performance on reward-guided unconditional protein sequence generation, over varying lengths and number of particles.

Data size	Joint Prompt Output	Product Prompt Output
N=10	The best estimate for parameters of the model are: $a = 4.337$, and $b = -34.049$	The best estimate for parameters of the model are: $a = 3.000$, and $b = 10.004$
N=20	Based on the observed data points, we can see a trend that y is directly proportional to x . The best estimate for the parameters a and b is: $a = 1.0$, and $b = 0.0$.	The best estimate for parameters of the model are: $a = 3.82$, and $b = 10.12$.
N=50	To obtain the best estimates for the parameters (a and b), you need to follow the detailed steps of building a linear regression model using Ordinary Least Squares (also namedIM, and guide, filter). These steps involve typically a program such as R or a statistical tool among others. The objective is to predict parameters, but after an ensemble calculation, we are going to use, known as the sum of residuals, to estimate the model's parameters. The sum of residuals helps us evaluate the discrepancy of model with a given residuals. Once I've made these predictions, I'll be able to provide more precise feedback on parameter estimates.	The best estimate for parameters of the model are: $a = 1.344$, and $b = -22.331$
N=100	The best estimate for parameters of the model are: $a = 0x583C622F 052D29A9 + 00EA6F242949D26F$ and $b = 0x 41796E30 0027A200 - 76CF406498D45505$. Note: These values of a and b are with 95% confidence taking into account the Gaussian balls added to Python and Python recovery points.	The best estimate for parameters of the model are: $a = 0.8313$, and $b = 0.0564$.

Table A3: Comparison between curated joint and product prompt outputs at varying data sizes.

Table A5: Maximum and average reward over unique sequences for protein tasks. (Average and standard error reported over all seeds for max reward, and over all sequences for the second column).

	Max $\log r(x)$ (\uparrow)	Avg. $\log r(x)$ on unique sequences (\uparrow)
Task: unconditional generation		
Base [unguided]	-2.4883 ± 0.3474	-4.4272 ± 0.1865
DG-Exact (Nisonoff et al., 2024)	-0.9119 ± 0.1508	-1.8831 ± 0.0979
FK Steering Singhal et al. (2025)	-2.4266 ± 0.3936	-2.9245 ± 0.1646
DFKC [ours]	-1.1797 ± 0.2507	-1.7642 ± 0.1554
Task: thermostability		
Base [unguided]	-0.4933 ± 0.0396	-0.6698 ± 0.0185
DG-Exact (Nisonoff et al., 2024)	-0.4404 ± 0.0322	-0.6122 ± 0.0181
FK Steering Singhal et al. (2025)	-0.4661 ± 0.0444	-0.5864 ± 0.0205
DFKC [ours]	-0.4266 ± 0.0311	-0.5388 ± 0.0170

Table A6: Ablation over number of SMC samples (M) for protein tasks (mean and standard error reported over 5 seeds).

	Reward		Diversity		Structural confidence			Novelty	
	$\log r(x)$ (\uparrow)	Seq. div. (\uparrow)	Max. cluster (\uparrow)	pLDDT (\uparrow)	pTM (\uparrow)	Frac. pLDDT > 0.7 (\uparrow)	Max TM (\downarrow)	Frac. TM < 0.5 (\uparrow)	
Task: unconditional generation									
Base [unguided]	-4.3266 ± 0.3190	0.7729	0.3571	0.5941 ± 0.1525	0.2609 ± 0.1452	0.2714	0.6789	0.0500	
FK Steering ($M = 5$) Singhal et al. (2025)	-3.3484 ± 0.1636	0.7054	0.1467	0.5896 ± 0.1505	0.2719 ± 0.1418	0.2467	0.7069	0.0808	
FK Steering ($M = 10$) Singhal et al. (2025)	-2.7662 ± 0.1160	0.6171	0.0733	0.5494 ± 0.1408	0.1912 ± 0.0845	0.2133	0.5992	0.1837	
DFKC ($M = 5$) [ours]	-1.6551 ± 0.0952	0.7077	0.1067	0.6005 ± 0.1840	0.2860 ± 0.1677	0.3600	0.6573	0.1443	
DFKC ($M = 10$) [ours]	-1.7380 ± 0.0577	0.6318	0.0667	0.5573 ± 0.1605	0.2387 ± 0.0775	0.2400	0.6536	0.0625	
Task: thermostability									
Base [unguided]	-0.6590 ± 0.0229	0.7729	0.3571	0.5941 ± 0.1525	0.2609 ± 0.1452	0.2714	0.6789	0.0500	
FK Steering ($M = 5$) Singhal et al. (2025)	-0.5841 ± 0.0192	0.7513	0.2733	0.5704 ± 0.1534	0.2246 ± 0.1087	0.2333	0.6559	0.1429	
FK Steering ($M = 10$) Singhal et al. (2025)	-0.5980 ± 0.0135	0.6944	0.2467	0.5473 ± 0.1495	0.1901 ± 0.0718	0.2000	0.5741	0.2024	
DFKC ($M = 5$) [ours]	-0.5316 ± 0.0153	0.7618	0.3200	0.5875 ± 0.1517	0.2468 ± 0.1387	0.2533	0.6490	0.2043	
DFKC ($M = 10$) [ours]	-0.5736 ± 0.0138	0.7554	0.3200	0.5866 ± 0.1451	0.2501 ± 0.1508	0.2600	0.6355	0.1096	